

# The entropy core in galaxy clusters: numerical and physical effects in cosmological grid simulations.

F. Vazza<sup>1\*</sup>

<sup>3</sup> INAF/Istituto di Radioastronomia, via Gobetti 101, I-40129 Bologna, Italy

Accepted ???. Received ???; in original form ???

## ABSTRACT

A flat distribution of low gas entropy in the core region of galaxy clusters is a feature commonly found in Eulerian cosmological simulations, at variance with most standard simulations of Smoothed Particles Hydrodynamics fashion. From the literature it is still unclear whether this difference is entirely due to numerical artifacts (e.g. spurious transfer from gravitational energy to thermal energy), to physical mechanisms (e.g. enhanced mixing in Eulerian codes) or to a mixture of both. This issue is related to many still open lines of research in the characterization of the dynamical evolution of the baryons in galaxy clusters: the origin of the cool core/non-cool core bi-modality, the diffusion of metals within galaxy clusters, the interplay between Active Galactic Nuclei and the Intra Cluster Medium, etc.

In this work, we aim at constraining at which extent the entropy core is affected by numerical effects, and which are the physical reasons for its production in cosmological runs. To this end, we run a set of 30 high resolution re-simulations of a  $\sim 3 \cdot 10^{14} M_{\odot}/h$  cluster of galaxies with a quiet dynamical history, using modified versions of the cosmological Adaptive-Mesh-Refinement code ENZO and investigating many possible (physical and numerical) details involved in the production of entropy in simulated galaxy clusters.

We report that the occurrence of a flat entropy core in the innermost region of massive cluster is mainly due to hydro-dynamical processes resolved by the numerical code (e.g. shocks and mixing motions) and that additional spurious effects of numerical origin (e.g. artificial heating due to softening effects) affect the size and level of the entropy core only in a minor way.

Using Lagrangian tracers we show that the entropy profile of non-radiative simulations is produced by a mechanism of “*sorting in entropy*” which takes place with regularity during the cluster evolution. The evolution of tracers illustrates that the flat entropy core is caused by *physical* mixing of subsonic motions (mostly driven by accreted sub-clumps) within the shallow inner cluster potential.

Several re-simulations were also produced for the same cluster object with the addition of radiative cooling, uniform pre-heating at high redshift ( $z = 10$ ) and late ( $z < 1$ ) thermal energy feedback from AGN activity in the cluster, in order to assess the effects of such mechanisms on the final entropy profile of the cluster. We report on the infeasibility of balancing the catastrophic cooling (and recovering a flat entropy profile) by means of the investigated trials for AGN activity alone, while for a sub-set of pre-heating models, or AGN feedback plus pre-heating models, a flat entropy distribution similar to non-radiative runs can be obtained with a viable energy requirement. Complementary analysis are presented also for a major merger cluster, obtaining similar results and achieving a generally good consistency with X-ray data for the entropy distribuion in real galaxy clusters.

**Key words:** galaxy clusters, ICM, turbulence, Adaptive Mesh Refinement, mixing, tracers

## 1 INTRODUCTION

The presence of a flat entropy core in the center of non-radiative galaxy clusters simulated with Eulerian grid codes, and its com-

plete absence in the core of galaxy clusters simulated with Lagrangian approaches (such as Smoothed-Particle-Hydrodynamics codes, SPH), has been object of an interesting debate in the last few years and among a number of different groups (e.g. Frenk et al.1999; Voit et al.2005; Dolag et al.2005; Lin et al.2006; Wadsley

\* E-mail: vazza@ira.inaf.it

et al.2008; Tasker et al.2008; Mitchell et al.2008; Springel 2010; Abel 2010).

The issue of the real inner entropy profile of non-radiative galaxy clusters may be loosely connected to the case of real clusters, which are interested by cooling and energy feedback by several astrophysical sources; nonetheless, this topic represents one of the main diagnostic to compare cosmological simulations of galaxy clusters performed with different numerical approaches.

The evolution of gas in the simulated Universe, when only shock heating is present as *explicit* source of energy dissipation, represents a rather simple scenario to study the thermodynamics of cosmic baryons starting from simple initial conditions. Understanding the systematics that affect the generation of entropy in the different codes, even in this rather idealized setup, would represent a useful step forward in all research topics dealing with the numerical treatment of non-reversible processes in astrophysical plasmas at all scales. In non radiative simulations of galaxy clusters, the task of understanding the correct entropy distribution in the innermost cluster regions is made complicated by a few circumstances: a) the radius of the entropy core produced in grid codes is rather small  $r_{core} \sim 0.1R_{vir}$  (where  $R_{vir}$  is the cluster virial radius), and even the most resolved cosmological simulations can concentrate only a moderate number of resolution elements, of the order of  $N \sim 10^2 - 10^4$ , inside this region: therefore resolution and sampling problems may always be present; b) the baryon accreted by a cluster are interested by several dynamical processes across their evolution (shock heating, violent relaxation, gas mixing and sloshing of the Dark Matter peak) which distribute entropy in clusters in different ways; disentangling the various effects within the same galaxy cluster is usually not a trivial task; c) due to the typical radial entropy distribution in galaxy clusters, *physical* mixing driven by matter sub-clumps in-falling from the outside regions, and *numerical* mixing or spurious heating from N-body noise would have the same net effect, leading to an increase of gas entropy within the densest regions in clusters; unluckily, the different numerical methods are prone to numerical mixing in a ways difficult to quantify. Therefore very similar entropy configurations may be degenerate respect to various interplays between physical and numerical effects along the whole cluster evolution, and specific numerical tests aiming at the close comparison between re-simulations of the same objects with different numerical methods are highly desirable in this respect.

From the literature, the first clear indication of a fundamental difference between the results of SPH codes and grid ones in galaxy cluster simulations was presented in the Santa Barbara Comparison project (Frenk et al.1999). In this work, evidence was obtained that the innermost entropy radial distribution in cluster simulated in grid methods such as ENZO contain a nearly isentropic core inside  $\sim 0.1R_{vir}$ , at variance with SPH codes; later works basically confirmed this trend also at higher resolutions (e.g. Voit et al.2005; Wadsley et al.2008). Several reasons were suggested to interpret this discrepancy: over-mixing in grid codes (e.g. Wadsley et al.2008), spurious N-body heating from DM particles in the cluster core (e.g. Lin et al.2006; Springel 2010), Galilean invariance in the gravity solver of grid codes (Tasker et al.2008; Robertson et al.2010), lack of physical mixing in SPH codes (e.g. Dolag et al.2005; Agertz et al.2007; Abel 2010), pre-shocking in SPH (e.g. O’Shea et al.2005) etc. To date, the most detailed analysis of the generation of entropy has been presented by Mitchell et al.(2009), by studying idealized cluster mergers with a non-cosmological setup with the SPH code GADGET2 (Springel et al.2005) and the

grid code FLASH (Fryxell et al.2000). The authors provided striking evidences that the mechanism at work in setting the different entropy level between SPH and grid codes takes place at the time of the closest encounter between the colliding structures, and it is related to the suppression of mixing in SPH because of artificial viscosity, which highly suppresses hydro instabilities and mixing motions respect to grid codes. It would be now interesting to extend the results of this seminal paper to fully cosmological simulations, and to the case of clusters in which the mass is assembled with realistic and different dynamical history (major mergers or regular smooth accretions).

The present paper is first devoted to constrain at which extent all the numerical effects cited above may affect also the specific distribution of gas entropy in realistic and high resolution cosmological simulations. Secondly, this paper is devoted to focus on the physical mechanisms for the generation and the spreading of gas entropy within clusters, in relation to gravitational mechanisms (e.g. shock heating and mixing motions) and to non-gravitational ones (e.g. radiative cooling and energy feedbacks from astrophysical sources such as AGNs). To this end we produced a set of 30 re-simulations of the same galaxy cluster, with a final mass of  $M \approx 3.1 \cdot 10^{14} M_{\odot}/h$  and a very quiet dynamical history for most of its evolution (complementary results for a major merger cluster are shown in the Appendix).

The first part of this work (Sec.3) explores many of the possible numerical mechanisms which may lead to the formation of an inner entropy core in *cosmological* cluster simulations, by using customized re-simulations with the adaptive mesh refinement code ENZO (Norman et al.2007). In detail, Sec.3.2 discusses the role of the mesh refinement strategy adopted in the simulation; Sec.3.3 estimates the role played by cold unresolved flows and N-body gravitational heating, making changes to the “dual energy formalism” method adopted in ENZO; Sec.3.4 investigates the influence of the softening length in the computation of the gravitational force in the PM method; Sec.3.5 compares re-simulations adopting different maximum resolution to compute hydro-dynamics of baryons.

In Sec.4.1 the *physical* generation of entropy and the volume spreading of it during cluster evolution is investigated by means of Lagrangian tracers, injected and evolved in non radiative runs.

Radiative cooling can completely alter the above picture, in systems characterized by a cooling time shorter compared to the cluster lifetime (e.g. Katz & White 1993; Fabian 1994). Indeed the hot gas phase in the core region of these systems is removed by the radiative losses, and the inward motion of the cooling gas would produce the theoretical “cooling flow” scenario. However, drastic cooling flows are not observed in real clusters, and additional *non-gravitational* heating mechanisms are need to restore (or keep) the cooling gas on an higher adiabat (e.g. Evrard & Henry 1991; Kaiser 1991; Lloyd-Davies, Ponman & Cannon 2000). Two of the most promising scenarios in this respect are the pre-heating scenario (e.g. White 1991), in which gas is heated before it collapses within structures, or AGN feedback (e.g. Churazov et al.2000), in which the inner entropy is raised by the energy released, through different channels, out of the regions surrounding the growing super massive black hole. Many works investigated the above mechanisms with cosmological simulations, by implementing non-gravitational heating mechanisms in SPH or in grid methods (e.g. Borgani et al.2002; Borgani et al.2005; Heinz et al.2006; Sijacki & Springel 2006; Younger & Bryan 2007; Burns et al.2008; Mc Carthy et al.2009; Teyssier et al.2010). However comparing the outcomes of these studies is made complex by the great number of assumption and

parameters often involved in the modelization of feedback sources. Also considering the underlying fundamental differences of the hydro methods discussed above, the characterization of the inner entropy profile of radiative cluster with non-gravitational heating mechanisms at play is a still very open topic of research for simulations. For instance, qualitatively similar models applied to GADGET (Borgani et al.2002) or ENZO simulations (Younger & Bryan 2007) has lead to different conclusion about the efficiency of pre-heating at the scale of galaxy clusters or galaxy groups. The ability of cluster merger in quenching (or slowing down) the cooling catastrophe in radiative simulations is also a debated issue (Burns et al.2008; Poole et al.2008).

In the second part of the paper (Sec.4) we focus on the additional *physical* mechanisms which are able to affect the gas entropy distribution in real galaxy cluster, by studying in detail the effects of a) radiative cooling (Sec.4.2); b) non-gravitational heating by a "uniform" heating mechanism in the early Universe (Sec.4.2.1); c) non-gravitational heating by a central AGN with outflows, within an already formed cluster (Sec.4.2.2-4.2.3). Our goal is not that of constraining the most likely extra heating mechanism at work in real galaxy cluster, but rather to show what is the net effect of *plausible* heating mechanism on the entropy distribution of a cluster with an ongoing cooling flow, using a budget for the energy release under control.

Section 5 finally summarizes our discussions of the results and our conclusions, while in the Appendix complementary tests studying the numerical and physical generation of entropy in major merger cluster are reported for completeness.

## 2 NUMERICAL CODE AND SETUP

The computations presented in this work were performed using the ENZO code, developed by the Laboratory for Computational Astrophysics at the University of California in San Diego (<http://lca.ucsd.edu>).

ENZO is an adaptive mesh refinement (AMR) cosmological hybrid code highly optimized for high performance computing (Norman et al.2007 and references therein). It uses a Particle-Mesh method to follow the dynamics of the collision-less Dark Matter (DM) component (Hockney & Eastwood 1981), and a Eulerian solver based on the Piecewise Parabolic Method (PPM, Woodward & Colella, 1984).

The adopted simulational setup is the same as in Vazza, Gheller & Brunetti (2010). In summary, cosmological initial conditions were produced with nested grid/DM particle distributions of increasing in order to achieve high DM mass resolution in the region of cluster formation; also an implemented mesh refinement scheme was applied to trigger mesh refinement based on gas/DM over-density and/or velocity jumps across cells. In this scheme, a normalized 1-D velocity jump across 3 adjacent cells in the scan direction (at a given refinement level) is recursively computed as  $\delta \equiv |\Delta v/v_{min}|$ , where  $|v_{min}|$  is the minimum velocity, in absolute value, among the 3 cells. The scheme is made manifestly non Galileian invariant by the presence of  $v_{min}$ ; this problem is unavoidable in this kind of simulations, because in principle every forming shock wave moves on a different reference frame, and a run-time procedure to account for this would represent a too large computational effort. In order to have this effect under control we performed many convergence tests with idealized and cosmological

**Table 1.** Main characteristics of the performed runs. Column 1: run identification code; column 2: cell resolution at the maximum refinement level; column 3: maximum softening length; column 4: mesh refinement strategy: "D"= gas/DM over-density refinement; "V"=velocity jumps refinement; column 5: additional numerical parameter of the simulations.  $\eta_1$ ,  $\eta_2$  and  $M_{thr}$  are parameters involved in the dual energy formalism switch (Sec.3.3); "PH" means that uniform pre-heating has been adopted, assuming an entropy increase of  $S_0$  at  $z = 10$ ; "J" means that  $\epsilon_{jet}$  extra energy has been injected at  $z \leq 1$  within the cluster, assuming AGN feedback.

ID	Max Res. [kpc/h]	$\epsilon_{soft}$ [kpc/h]	AMR	note
R0	25	50	DV	non-radiative
R1	25	25	DV	non-radiative
R2	25	50	D	non-radiative
R3	25	25	D	non-radiative
R4	12.5	25	DV	non-radiative
R5	12.5	25	D	non-radiative
R6	12.5	12.5	DV	non-radiative
R7	12.5	12.5	DV	non-radiative
R18	25	100	D	non-radiative
R19	25	100	DV	non-radiative
R20	25	12.5	D	non-radiative
R21	50	50	D	non-radiative
R22	50	50	DV	non-radiative
R8	25	25	DV	$\eta_1 = 10^{-2}$
R9	25	25	DV	$\eta_1 = 10^{-4}$
R10	25	25	DV	$\eta_2 = 1$
R11	25	25	DV	$\eta_2 = 10^{-2}$
R12	25	25	DV	$M_{thr} = 1.1$
R13	25	25	D	$M_{thr} = 1.5$
R15	25	25	DV	cooling
R16	25	25	D	cooling
PH1	25	25	DV	cool.+PH( $10keVcm^2$ )
PH2	25	25	DV	cool.+PH( $100keVcm^2$ )
PH3	25	25	D	cool.+PH( $100keVcm^2$ )
PH4	25	25	DV	cool.+PH( $200keVcm^2$ )
B1	25	25	DV	cool.+J( $10^{58}ergs$ )
B2	25	25	DV	cool.+J( $10^{59}ergs$ )
B3	25	25	D	cool.+J( $10^{59}ergs$ )
B4	12.5	12.5	DV	cool.+J( $10^{58}ergs$ )
B5	25	25	DV	cool.+PH+J( $2 \cdot 10^{57}ergs$ )

simulations with ENZO, finding showing that a very good numerical convergence is achieved in cluster simulations by fixing  $\delta = 3$  (more detailed discussions can be found in Vazza et al.2009; Vazza, Gheller & Brunetti 2010).

All the re-simulations presented here focus on the evolution of the same galaxy cluster, which was the most massive one of the sample already presented in Vazza, Gheller & Brunetti (2010).

In order to role of various numerical effects (such as resolution, softening in the gravitational force, etc.) various re-simulations starting with the same initial conditions were produced. Table 2 lists the details of all runs performed for this project. The re-simulations employing additional physics (such as pre-heating and AGN feedback) where produced with original implementations made starting from the public 1.5 version of ENZO.

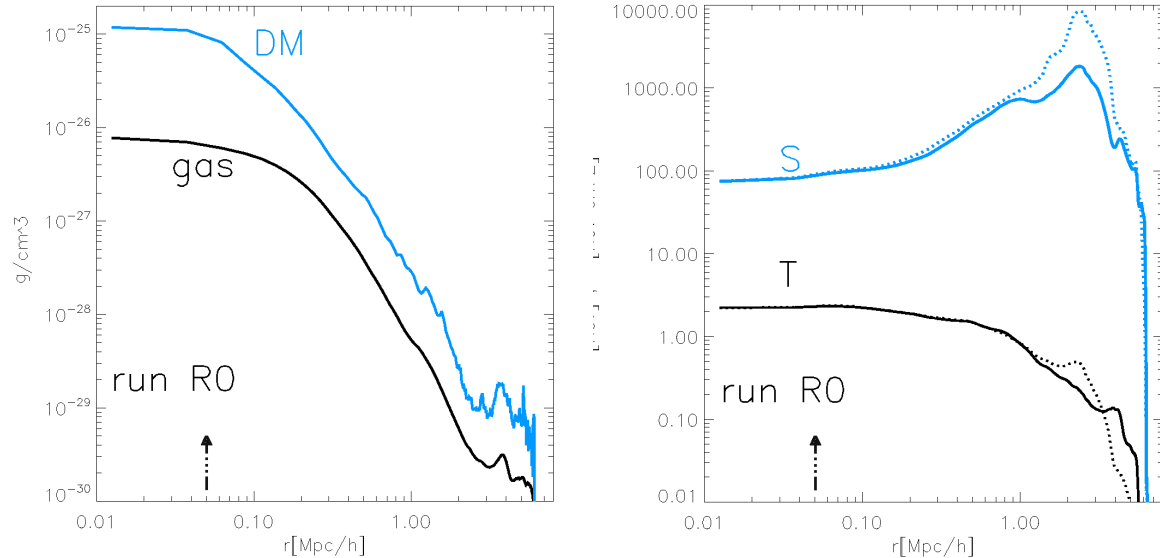


**Figure 3.** Radial profiles for the run R0, showing gas density and DM density profiles (left panel) and gas temperature and gas entropy (right panel). In the right panel, the solid lines refer to mass-weighted profiles, while the dashed lines refer to volume-weighted profiles. The vertical arrows show the softening length adopted in this run.

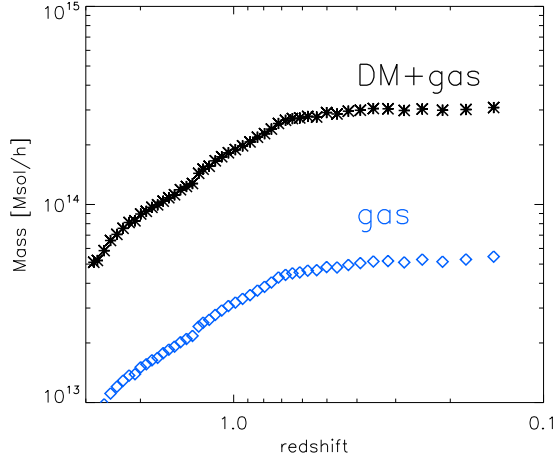


**Figure 1.** Redshift evolution of the Dark matter plus gas mass (black), and of total gas mass (blue) inside the virial radius of the galaxy cluster studied in this work.

### 3 NUMERICAL EFFECTS ON THE ENTROPY PRODUCTION.

#### 3.1 The fiducial run

The fiducial cluster run of this project is R0, which has the same numerical setup and mesh refinement strategy already adopted in other works by our group (Vazza et al.2009; Vazza, Gheller & Brunetti 2010; Vazza et al. 2010). The assumed cosmology is the “Concordance”  $\Lambda$ CDM model, with parameters:  $\Omega_0 = 1.0$ ,  $\Omega_{BM} = 0.0441$ ,  $\Omega_{DM} = 0.2139$ ,  $\Omega_{\Lambda} = 0.742$ , Hubble parameter  $h = 0.72$  and a normalization for the primordial density power spectrum  $\sigma_8 = 0.8$ . The mesh refinement on gas/DM over-density is triggered since the beginning of the simulation inside a cubic

with the side of  $\approx 5R_{vir} \approx 12Mpc/h$ <sup>1</sup>,  $z = 30$ , while the additional mesh refinement triggered by velocity jumps is activated from  $z = 2$ .

The lowest resolution level ( $l = 0$ ) inside the AMR region is  $220kpc/h$ , while the maximum refinement level ( $l = 3$ ) is set to  $25kpc/h$ . The DM matter particles have a mass resolution of  $6.7 \cdot 10^8 M_{\odot}/h$ , and the comoving gravitational softening is  $\epsilon = 50kpc/h$ .

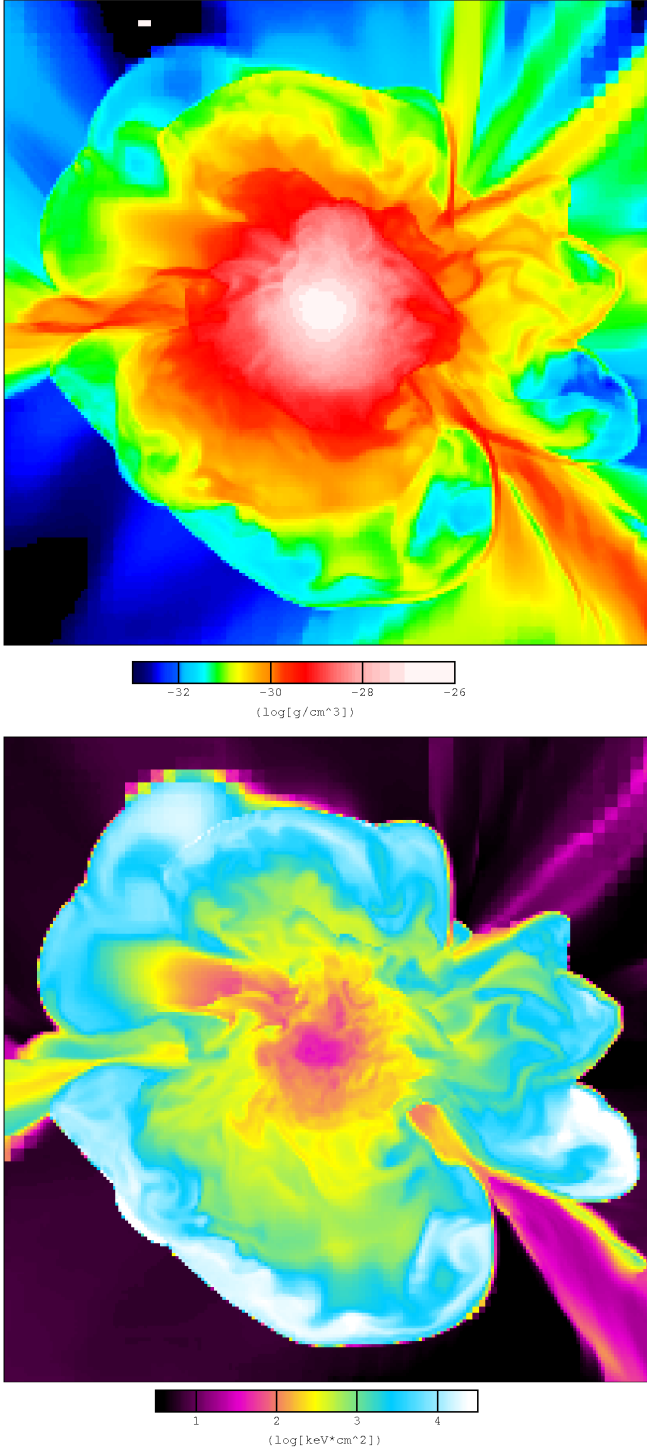
This fiducial cluster run does not include radiative cooling or any heating mechanism other than gravitational collapse or shock heating.

Fig.1 shows the redshift evolution of the total mass and of the gas mass inside the virial cluster region, measured with a spherical over-density method. The trend of the cluster mass growth and the visual inspection of movies of its evolution confirms that this cluster does not experience any violent merger event for  $z < 1.5$ , and roughly  $\sim 70$  per cent of its mass has been already assembled at  $z \sim 0.6$ . At  $z = 0$  the cluster has a total mass of  $\approx 3.1 \cdot 10^{14} M_{\odot}/h$ , an average temperature of  $2.2keV$  and a virial radius of  $R_v = 1.89Mpc/h$ .

In Fig.2 we show the maps of gas density and gas entropy<sup>2</sup> through the center of the cluster. The cluster is quite regular in shape, with sharp circular shock structures and a well defined inner entropy floor of size  $r_{core} \sim 100kpc/h$  surrounded by the steep increase of the ICM entropy, up to a maximum at about  $\sim 2Mpc/h$  from the cluster center. This cluster may be considered as a “prototype” of relaxed clusters in the local Universe with intermediate mass, as produced by non-radiative cosmological simulations of Eulerian fashion. For complementary results on larger mass clus-

<sup>1</sup> In the following, we will refer to this region as to the ‘AMR region’.

<sup>2</sup> All throughout this paper, we will refer to  $S \equiv \frac{P}{\rho^{\gamma}}$  as to the “gas entropy”, as usually done in cosmological numerical simulations, where  $P$  is the gas pressure,  $\rho$  is the gas density within a cell and  $\gamma$  is the adiabatic index.



**Figure 2.** Maps of gas density (*top*) and gas entropy (*bottom*) for a slice crossing the center of the cluster at  $z = 0$  (run R0). The side of the image is  $\approx 5.5 Mpc/h$  and the width of the slice is one cell =  $25 kpc/h$ .

ters simulated with the same approach, we refer the reader to recent high-resolution re-simulations presented in Vazza et al.(2010), and references therein.

Figure 3 shows the radial profiles of gas density, DM density, temperature and entropy for run R0 at  $z = 0$ . In the right panel of this Figure we compare gas mass weighted profiles and volume weighted profiles for the cluster run: the two estimates pro-

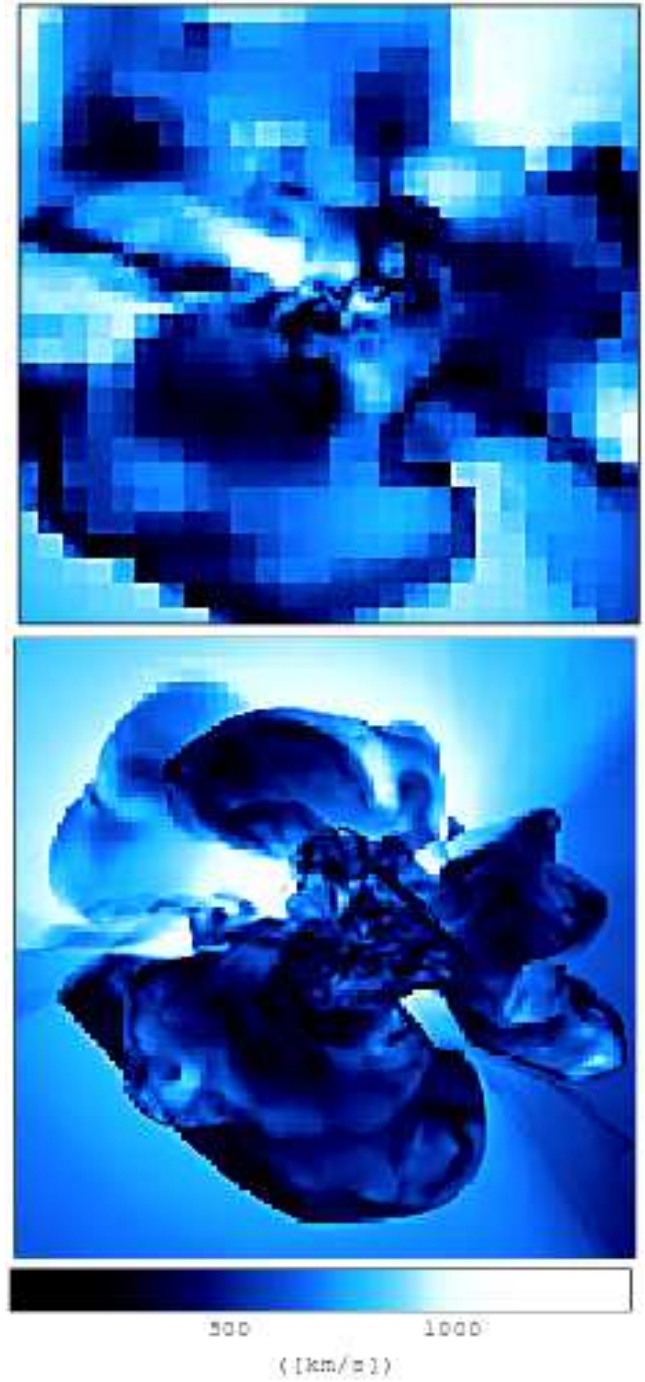


**Figure 4.** Slices showing the absolute value of the 3-D velocity field for run R0 (Top panel) and run R2 (Bottom panel) at  $z = 0$ . The size of the image is as in Fig.2.

vide consistent results within  $< 2 Mpc/h$  from the cluster center. Unless specified, in what follows we will make use of gas density weighted averages.

We investigated the “robustness” of this cluster representation by adopting several changes in this simple setup, which will be discussed in the next Sections.

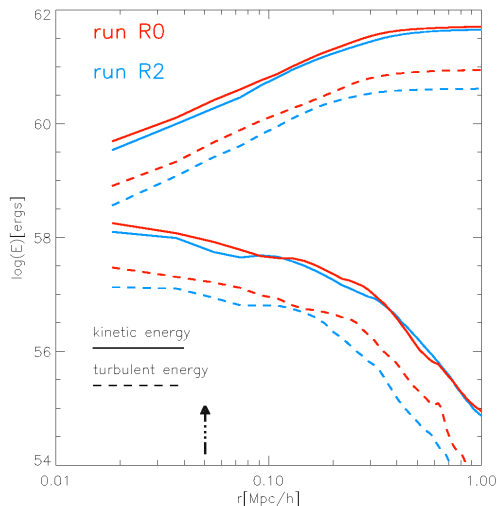


**Figure 5.** Radial profiles of kinetic energy for run R0 (red solid) and for run R2 (blue solid), and of “turbulent” kinetic energy for the same runs (dashed lines). The 4 top lines refer to the total kinetic/turbulent energy inside a given radius, while the 4 bottom lines refer to the values within shells of width  $25kpc/h$  at the same radii. The vertical arrow shows the softening length adopted in these runs.

### 3.2 The role of the mesh refinement strategy.

Shock heating during the gravitational collapse in the forming cluster has a leading role in the production of the baseline entropy distribution within clusters, since no other *physical* mechanisms of irreversible heating are present in simple non-radiative cosmological simulations (e.g. Voit et al.2005). Previous works in the literature (Dolag et al.2005; Iapichino & Niemeyer 2008; Vazza et al.2009; Vazza, Gheller & Brunetti 2010) have suggested that an increase of the level of chaotic motions within simulated clusters is expected as soon as the effects of a coarse resolution or artificial viscosity are limited by ad-hoc techniques, and as a result typically higher entropy level is found in the core region of cosmic structures. Also, the different ability in modeling shocks and mixing in the central phase of cluster mergers has proved to be responsible for the bulk of the difference between SPH or grid simulations of galaxy clusters (Mitchell et al.2009). Obtaining a good spatial resolution of chaotic and mixing motion in the ICM is therefore crucial and the mesh refinement strategy outlined in Sec.3.1 is designed for this purpose (see also Iapichino & Niemeyer 2008).

We compare the cluster entropy profile in the fiducial run (R0) against a re-simulation using the standard mesh refinement based on gas/DM over-density alone (run R2). Figure 4 shows the maps of the absolute value of the velocity field in the two runs, for a slice crossing the center of the cluster at  $z = 0$ . Similarly to what reported in Vazza et al.(2009), the extra refinement strategy allows us to preserve a very accurate description of the low density outer accretion region, and on the mixing motions following the crossing of satellites even if the involved over-density is not enough to trigger other refinements. The radial distributions of the kinetic energy and “turbulent” energy (we fiducially consider as “turbulent” the components of the 3-D velocity field which are characterized by a coherence scale smaller than  $< 200kpc/h$ , see Vazza et al.2009 Sec.4.2 for further details) are shown in Fig.5. As expected, R0 shows a slightly higher level of kinetic energy all across the cluster

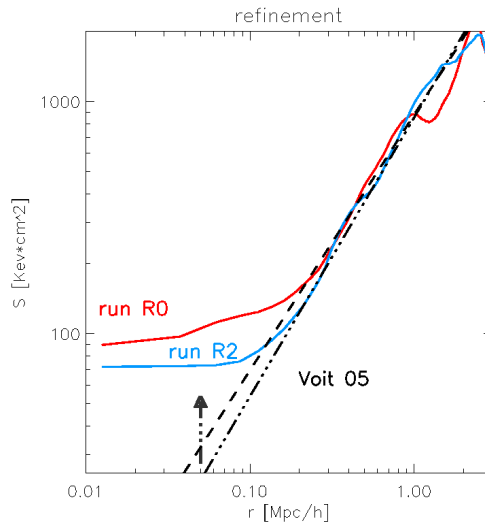


**Figure 6.** Gas entropy profile for run R0 (red) and run R2 (blue). The additional black lines show the fit profiles presented in Voit et al.(2005), for  $S \propto r^{1.1}$  (dashed) and  $S \propto r^{1.2}$  (dot-dashed). The vertical arrow shows the softening length adopted in these runs.

volume, and an kinetic energy in small-scale chaotic motions by a factor  $\sim 2 - 3$  compared to the standard run R2.

The entropy profiles of the two simulations are shown in Fig.6. The additional black lines show the fit profile presented in Voit et al.(2005), where a systematic study of entropy profile in non-radiative cluster simulations (of SPH and grid fashion) were presented. The run with the additional refinement strategy produces a significantly larger entropy within the core region, by a  $\sim 20 - 30$  per cent (the gap is  $30 - 50keVcm^2$ ). It is interesting to notice that the gas entropy and the gas kinetic/turbulent energy of run R0 is larger compared to run R2 within approximately the same radius,  $r < 200kpc/h$  (the softening for the gravitational force here is  $50kpc/h$  at the maximum refinement level).

Already from this, one would speculate that enhanced turbulent mixing motions are responsible for the level of gas entropy inside clusters; we will focus on this issue with more detail in Sec.4.

### 3.3 The role of gravitational N-body heating and cold unresolved flows.

It has been suggested in the recent past that the entropy core in grid simulation may be due to an incorrect handling of the gas thermal energy/entropy, in the case of poorly resolved cold flows dominated by kinetic energy (e.g. supersonic flows in the rarefied Universe) and due to noise-induced heating in virialised structures (Lin et al.2006; McCarthy et al.2007; Springel 2010). This second mechanism may arise because the small-scale velocity fluctuations induced by the N-body gravitational field can be readily dissipated by the mesh-based hydrodynamics, causing a spurious heating of the gas. In Springel (2010) the initial conditions for the Santa Barbara Comparison (Frenk et al.1999) were evolved with the AREPO code using an energy-entropy switch scheme in order to decide if the gas entropy had to be updated as the difference between the total energy and the kinetic energy (as customarily done in grid codes) or by directly using the entropy equation instead. This was done in order to ensure that in the case of transonic or subsonic motions ( $M < M_{thresh}$ , with  $M_{thresh} = 1.1$ ) the evolution of gas entropy

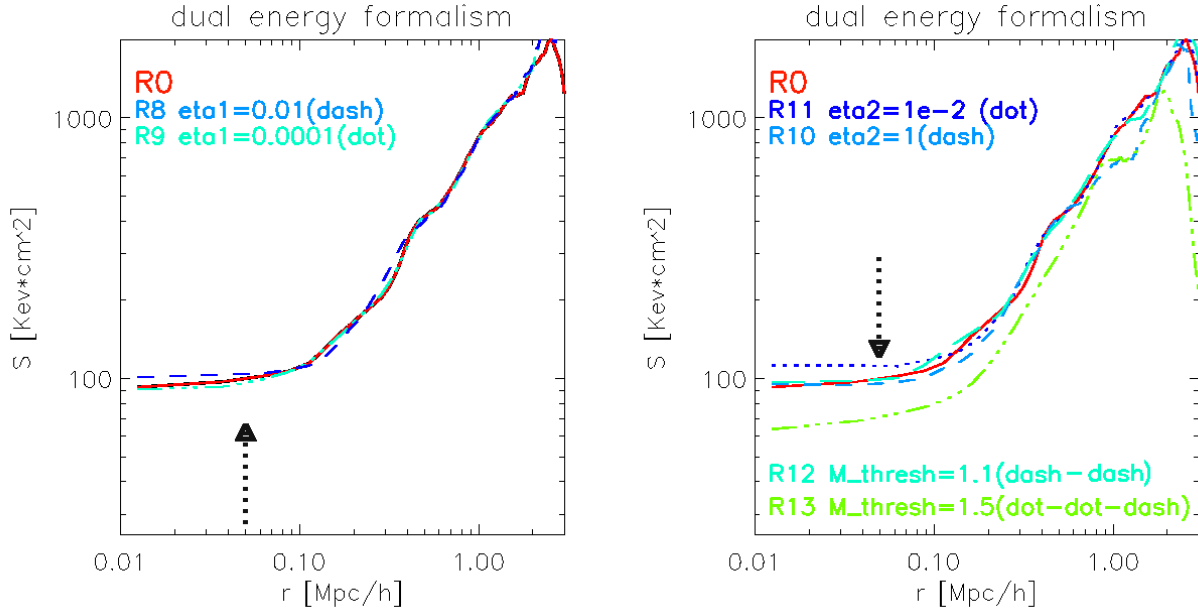


**Figure 7.** Comparison of the entropy profiles for different choices of the  $\eta_1$  (R8,R9, left panel) and for different choices of  $\eta_2$  (R10,R11, right panel). Additional green profiles are shown for ENZO re-simulations which adopted an additional switch condition on the Mach number to trigger the dual energy formalism (R12,R13). The vertical arrow in both panel shows the softening length adopted in these runs.

was not dominated by any spurious dissipation, since a *conservative* entropy equation was followed. The level of core entropy in the simulated cluster was found to be considerably reduced after the use of this switch, and the conclusion was that the entropy in the core region of clusters simulated with standard methods in grid simulations may be significantly affected by this numerical effect.

This issue is very interesting and deserves investigation; to this end we re-simulated run R0 with different choices for the computation of gas thermal energy. The strategy customarily adopted in ENZO is to adopt a “dual energy formalism” (Ryu et al.1993; Bryan et al.1995) designed to compute the evolution of gas thermal energy whenever the internal energy,  $e$ , cannot be calculated correctly as the difference between total,  $E$ , and kinetic energy (due to the fact that  $E \gg e$  in highly supersonic flows, and round-off errors may dominate). We briefly recall here its design: a first switch condition is followed to update the gas pressure in the case of very cold flows

- $p = \rho(\gamma - 1) \cdot (E - v^2/2)$  if  $(E - v^2)/E > \eta_1$
- $p = \rho(\gamma - 1) \cdot e$  if  $(E - v^2)/E < \eta_1$

where  $p$  is the gas pressure,  $v$  is the modulus of the velocity field and  $\gamma = 5/3$ . The second switch is adopted to update the internal gas energy without advecting numerical errors from each cell’s local neighborhood:

- $e = (E - v^2/2)$  if  $\rho(E - v^2)/\max[\rho E]_{neigh} > \eta_2$
- $e = p/\rho(\gamma - 1)$  if  $\rho(E - v^2)/\max[\rho E]_{neigh} < \eta_2$ ,

where  $\max[\rho E]_{neigh}$  is the maximum total energy in the (1-D) neighborhood of the cell. This approach ensures that  $e$  is not contaminated by errors advected by the total energy formulation (Bryan et al.1995). However we note that in the above switch conditions the presence of  $v$  makes them non Galileian invariant, because bulk velocities affect the exact value of  $E$  and of  $\max[\rho E]$ . To keep this problem under control, one need to resort to convergence studies by varying the numerical parameters involved in the

switch; the customary values set in ENZO cosmological simulations are  $\eta_1 = 10^{-3}$  and  $\eta_2 = 0.1$ .

As a first step to investigate the role played by the dual energy formalism in the production of the entropy level in clusters, we performed several tests by re-simulating the fiducial run adopting different choices of the threshold values involved in the above “switches”:  $\eta_1 = 10^{-2}$  (R8),  $\eta_1 = 10^{-4}$  (R9), or  $\eta_2 = 1$  (R10),  $\eta_2 = 10^{-2}$  (R11).

The motivation for this kind of tests is that if the low entropy gas sitting in the cluster center at  $z = 0$  is reminiscent of the entropy production prior to the cluster virialization, then any artifact present in the “cold” ( $T < 10^5 K$ ) Universe at early redshifts (i.e. due to an incorrect handling of the gas internal energy, or to features related to non Galileian invariance) will be highlighted by different choices of the entropy switch. It should be noted that, in absence of a re-heating UV background due to stars/AGN (e.g. Haardt & Madau 1996), the baryon temperature outside structures can be as low as  $T \sim 1 - 10 K$  in simulation of this kind.

By comparing the results of these runs with the fiducial one, we report that the net effect of the above changes is quite small, as shown in Fig.7: the maximum difference is found for run R11 ( $\eta_2 = 10^{-2}$ ) and results only in a  $\sim 10$  per cent larger entropy inside the cluster core. Cold unresolved flows are unlikely to be the reason of the entropy core in grid simulations.

As a second step to investigate further the possible role played by weak shocks and extra-heating related to N-body gravitational noise, we supplemented the dual energy formalism in ENZO with an additional Galileian-invariant switch based on the Mach number, with a procedure similar to Springel (2010).

As shown above the standard switch condition of the dual energy formalism may be affected by the presence of large bulk velocities, which enter in the total energy  $E$ , and thus the value of the parameter  $\eta_2$  cannot be readily related to the real Mach number of the flow. For this reason we implemented an on-the-fly shock in

ENZO simulations, which allows us to apply a Galileian invariant switch condition (based on the Mach number) to decide whether or not the total energy equation must be used to update the gas dynamics. This method relies on the temperature jumps method of Ryu et al.(2003) and adopts the following procedure: a) candidate shocked cells are identified according to the  $\nabla \cdot \vec{v} < 0$  criterion; b) local gradients of gas entropy,  $\nabla S$  and gas temperature  $\nabla T$  are evaluated, and a shock condition is matched whenever  $\nabla T \cdot \nabla S > 0$ ; c) the shock Mach number is estimated by inverting the maximum temperature jump across the shocked cell:

$$T_2/T_1 = \frac{(5M^2 - 1) \cdot (M^2 + 3)}{16 \cdot M^2}. \quad (1)$$

This procedure is followed on the fly during the simulation, and in this method the total energy equation is used to compute the gas internal energy only when  $\rho(E - v^2)/\max[\rho E]_{neigh} < \eta_2$  and  $M < M_{thresh}$  simultaneously. This procedure forces the code to update the gas thermal energy only in an adiabatic way, for flows with  $M < M_{thr}$ ; however we note that this formulation is not totally equivalent to the energy-entropy formalism discussed in Springel (2010), because the internal energy equation does not explicitly conserve gas entropy (however it conserves gas energy). The internal energy equation only depends on the second order of the gravitational potential,  $\Phi$ , through the coupling with the gas velocity field,  $\sim \nabla v \sim \nabla^2 \Phi$ , and therefore in this way the bulk of the (possible) N-body noise heating should be greatly reduced.

We performed two re-simulations of R0 adopting  $M_{thr} = 1.1$  (R12) and  $M_{thr} = 1.5$  (R13) (long dashed lines in the right panel of Fig.7).

We verified the difference in the total number of cells advanced with the total energy equation in the standard switch ( $\eta_2$  condition) or with the new switch ( $M_{thr}$  condition) by applying the two methods to the same snapshot of the R0 run, at  $z = 2$  and  $z = 1$ . We found with the first approach the number of cells advanced with the total energy equation is  $\sim 70$  ( $\sim 63$ ) per cent of the total in the AMR regions at at  $z = 2$  ( $z = 1$ ); with the  $M_{thr} = 1.1$  condition this ratio is decreased to  $\sim 50$  ( $\sim 45$ ) per cent of cells at  $z = 2$  ( $z = 1$ ), and with  $M_{thr} = 1.5$  the ratio is  $\sim 40$  ( $\sim 30$ ) per cent of cells at  $z = 2$  ( $z = 1$ ).

When the switch conditions on the Mach number are applied since the beginning of the cluster simulation, the run with  $M_{thr} = 1.5$  (run R13) shows a significantly reduced (by a factor  $\sim 50$  per cent) entropy production at all radii from the cluster center, but yet producing a very flat entropy distribution for  $r < 0.1R_{vir}$ . However run R13 shows a nearly constant decrease of entropy at *all* radii from the cluster center compared to all the other runs. Considering that the distribution of thermalized energy at shocks in our galaxy clusters simulations is a very steep function of  $M$ , with a well defined peak around  $M \sim 2$  (e.g. Vazza, Brunetti & Gheller 2009; Vazza et al.2010), the filtering procedure of run R13 is expected to filter out a  $\sim 50$  per cent of the energy input from cosmological shocks. Therefore this explains why the large value of  $M_{thr} = 1.5$  removes a significant part of the *genuine* production of entropy at cosmological shocks, and suggests that the entropy level found in the other run is mainly produced by the action of *physical* shocks dissipation.

When the Mach number for the switch is set to the same value used by Springel (2010),  $M_{thr} = 1.1$  (run R12), the final entropy profile of our cluster is found to be nearly identical to the fiducial run, with a very similar flat entropy core. This is somewhat at variance with the findings reported in Springel (2010), where spurious entropy production was masked out by applying the  $M_{thr} = 1.1$

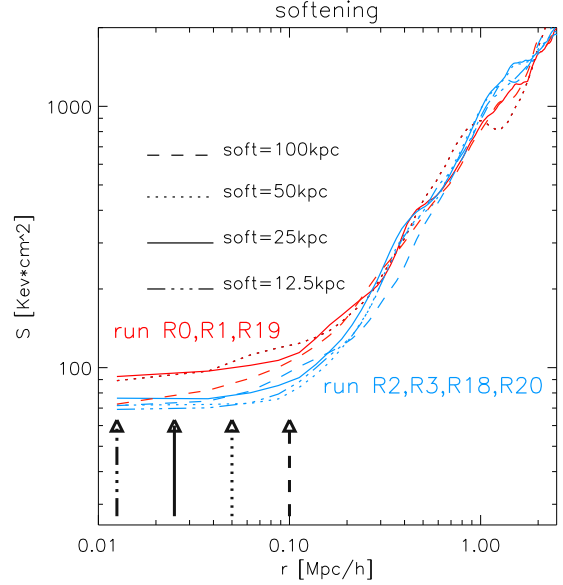


**Figure 8.** Comparison of the profiles obtained for different choices of the gravitational softening adopted in the N-body calculation (solid lines:  $\epsilon_{soft} = 50kpc/h$ ; dotted lines:  $\epsilon_{soft} = 25kpc/h$ ) for run adopting the standard refinement (R2,R3) or the velocity based one (R0,R1). The vertical arrows show the softening length of the various runs.

condition. A possible explanation for this may be related to the different on-the-fly strategies adopted to compute in run-time the Mach numbers between cells; further tests (also using other grid-based codes) may help to understand at which extent the exact formulation of the Mach number switch can be crucial to monitor the production of artificial entropy in cosmological cluster simulations.

To summarize what provided by our tests with ENZO AMR, the choice of the flow Mach number to decide whether or not the total energy must be used to evolve the gasdynamics of cells, is found to affect the *normalization* of the cluster entropy profile at  $z = 0$ , but not the *shape* of the distribution (at least for the  $M_{thr} \leq 1.5$  cases examined). Therefore the flat entropy core seems a pretty stable feature produced by ENZO AMR runs, and does not seem strongly affected by the details of the formalism adopted for the dual energy equation. At the present stage, we consider unlikely that the numerical issues discussed above can be fully responsible for the well known difference in the entropy profiles measured according to SPH or to grid methods.

### 3.4 The role of the smoothing in the gravitational force.

ENZO uses a particle-mesh N-body method (PM) to follow the dynamics of collision-less systems (e.g. Hockney & Eastwood 1981). DM particles are distributed onto a regular grid using the cloud-in-cell (CIC) interpolation technique, forming a spatially discretized DM density field. The DM density is then sampled onto the grid and the baryon density (calculated in the hydro method of the code) is added, and the gravitational potential is calculated on the periodic root grid using Fast Fourier Transform algorithms to solve the elliptic Poisson's equation. Since the acceleration is the gradient of the potential, the values of two potentials in close cells are required to calculate it, and thus the effective force resolution is about twice of the cell size. To calculate more accurate potentials on sub grids in the case of adaptive mesh refinement, the DM distribution is resam-



pled onto the finer grids using the same CIC scheme as for the root grid. The new boundary values are obtained with the interpolation from the gravitational potential on the parent grid, and a multirelaxation technique is used to obtain the gravitational potential at every point within the sub grids (e.g. O’Shea et al.2005).

The softening length,  $\epsilon_{soft}$ , used to compute the gravitational force and to update the DM particle motions is bound to be a multiple of the cell size. In ENZO  $\epsilon_{soft}$  can be as small as the finest refinement level in the volume, or an integer multiple of this.

Since the size of the entropy core is usually not much larger than the typical values of  $\epsilon_{soft}$  found in the innermost cluster region of most of AMR simulations, it is possible that the entropy core is an artifact due to the fact that for scales smaller than  $\epsilon_{soft}$ , the gravitational force does not longer obey the  $\propto 1/r^2$  scaling, but the  $\propto 1/(r + \epsilon_{soft})^2$  scaling instead<sup>3</sup>.

We investigated this issue by producing a several runs with identical initial but varying the minimum allowed  $\epsilon_{soft}$  to compute gravity forces. For the the velocity-based refinement, we compared the fiducial run R0 with run R1 ( $\epsilon_{soft} = 25kpc/h$ ) and with run R19 ( $\epsilon_{soft} = 100kpc/h$ ); for the standard refinement scheme, we compared run R2 with run R3 ( $\epsilon_{soft} = 25kpc/h$ ), with run R18 ( $\epsilon_{soft} = 100kpc/h$ ) and with R20 ( $\epsilon_{soft} = 12.5kpc/h$ ). Figure 8 shows that for a softening length of  $\epsilon_{soft} \leq 50kpc/h$  the flat entropy profile is a well converged feature in this cluster run, within a scatter of a 10 per cent at most, which may be due to slightly different timings in the different runs. For all softening smaller than  $\epsilon_{soft} = 50kpc/h$ , we also confirm that the two mesh refinement scheme always produce well separated entropy floor inside  $r < 200kpc/h$ . For the sake of completeness, the same analysis has been repeated in the case of a major merger cluster (see Appendix), leading to consistent results.

Mitchell et al.(2009) performed similar tests using FLASH, and also reported that the resolution used to compute gravity forces does not play an important role in setting the entropy profile inside the cluster, at least for maximum  $\epsilon_{soft} < 40kpc$ .

In general, we conclude that the flat entropy core in AMR simulations is not due to spatial undersampling of the gravity forces, and that the flat entropy core is observed even when  $\epsilon_{soft} \sim 0.05 - 0.1r_{core}$  (as in run R20). We thus conclude that the entropy core in grid simulation is not dependent on the adopted gravitational softening, for minimum softening length of  $50kpc/h$  or smaller.

### 3.5 The role of gas resolution.

The maximum cell resolution adopted to compute the hydrodynamical equations may play a role in setting the entropy content of a galaxy clusters, modifying the dynamics and propagation of shocks waves and modifying the evolution of chaotic motions in the ICM. The distribution of shocks energy and Mach number in grid codes is a quite regular function of the underlying grid resolution (e.g. Ryu et al.2003; Vazza, Brunetti & Gheller 2009). The average Mach number responsible for most of the thermal energy dissipation is a well converged quantity, for grid resolutions better than  $\sim 500kpc$ , even if the exact distribution of the high Mach number ( $M > 10$ ) tails is dependent on the underlying grid resolution.

However in the tests usually found in the literature for grid

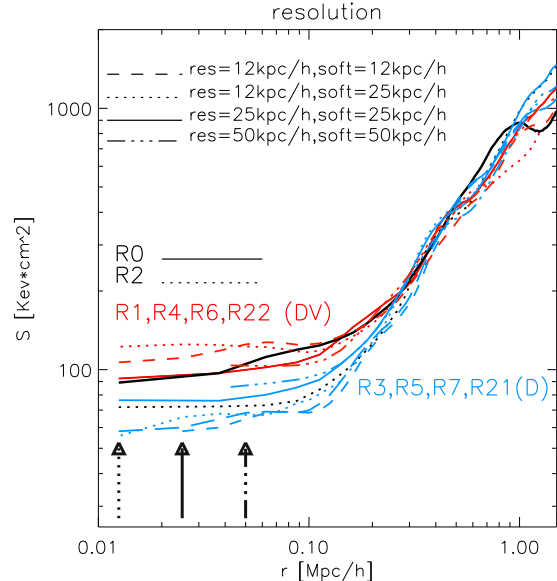


**Figure 9.** Overview of the effects of gas resolution and gravitational softening in the re-simulations. Red lines: runs adopting the velocity-based refinement (R1,R4,R6). Blue lines: runs adopting the overdensity-based refinement (R3,R5,R7). The additional black lines are for the fiducial run (R0, solid line) and for run R2 (dotted line). The vertical arrows show the softening length of the various runs.

simulations the above dependence is coupled with the dependence on  $\epsilon_{soft}$  (which may also indirectly affect the production of shocks by changing the morphology of in-falling gas/DM sub-clumps). We aim here to disentangle the two effects, by keeping the maximum softening length fixed to  $\epsilon_{soft} = 25kpc/h$ , but varying the maximum gas resolution in the computation of fluid-dynamical effects.

In runs R1 and R3 we allow ENZO to refine up to one level more,  $l = 4$ , keeping the same setup and refinement strategy of runs R4 and R5, respectively. If we compare the solid lines in Fig.9 (run R1,R3) and the dotted lines (run R4,R5) we see that the trend with gas resolution is opposite in the two mesh refinement strategies: while in the velocity-based refinement the entropy inside  $r \sim 100kpc/h$  is *increased* by a  $\sim 20 - 30$  per cent (R4), in the case of the overdensity-based refinement the inner entropy is *decreased* by a similar amount. The gap in entropy inside  $r_{core}$  is of the order of  $\Delta S \sim 30 - 60keV cm^2$ . We also re-simulated runs R4 and R5, allowing the code to increase also the softening length up to  $l = 4$  (run R6, R7, long dashed lines): the reported trends are the same (see red and blue dashed lines in Fig.9). The re-simulations shows that the difference between the two refinement schemes is always significant: a very flat entropy core inside  $r < 100kpc/h$  is produced in both cases, but a significant gap is found when comparing the two strategies, with the implemented refinement scheme producing the larger value. The trend is confirmed also by the comparison of two runs where the minimum softening and cell resolution were fixed to  $l = 2$  ( $50kpc/h$ ), run R22 and run R21 (dot-dashed lines in the same panel).

The reason for the *opposite* trend in the velocity-based scheme can be understood by the increased role of mixing motions, which cause a slightly more efficient inward transport of higher entropy material from the cluster outskirts (see also Sec.4). The efficiency of this mechanism is expected to increase as resolution is increased, since the velocity-based strategy is explicitly designed

<sup>3</sup> We note that however in recent ENZO AMR re-simulation of more massive galaxy clusters the scale of the entropy core is found to be  $\sim 10$  larger than the gravitational softening (Vazza et al.2010).

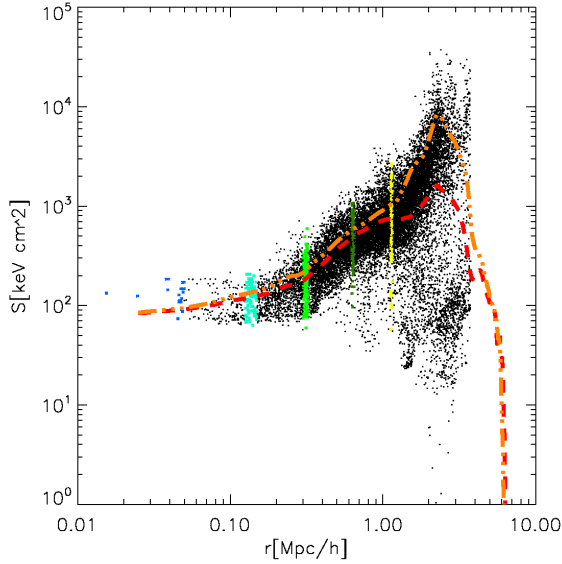


**Figure 10.** Radial entropy distribution for all  $N = 10^5$  tracers evolved in run R0. The colored sub sample shows the selections used for tests in Sec.4.1. The additional lines show the average entropy profile of the cluster (red/dashed:gas density weighted profile; orange/dot-dashed: volume-weighted profile).

to reduce the artificial dampening of small scale chaotic motions, which are partly responsible of diffusive mixing in the ICM. In the overdensity-based approach *clumps* are refined more and more, and they can deliver low entropy gas in the innermost region in a more efficient way; an increase of resolution also minimizes the effect of numerical mixing and let the cold gas phase to survive longer (e.g. Wadsley et al.2008; ZuHone, Markevitch & Johnson 2009). On the other hand in the velocity-based strategy the clumps are also more refined, but they are also more efficiently destroyed, before reaching the cluster center, by ram-pressure stripping at the outer regions and excite chaotic motions which are more long-living since they are not damped by the code; the net effect is an increase of entropy inside  $r_{core}$  in the velocity-based strategy. This stresses the need of having an accurate description of shocks and turbulent motions of the ICM, since the inner entropy distribution does not only depend on the maximum resolution within the core, but also on the resolution at the outer regions, where the bulk of the cluster entropy is produced. Convergence tests reported in Mitchell et al.(2009) and in ZuHone, Markevitch and Johnson (2009) suggest that full convergence for the entropy profile in the standard refinement strategy is reached for a maximum resolution of  $\sim 10kpc/h$  or smaller. A similar conclusion is likely also the velocity-based strategy, but we could not run so far a re-simulations reaching  $l = 5$  for computational limitations. However the trend of the red lines in Fig.9 suggest that convergence is near.

We conclude that even if the different mesh refinement strategies and the adopted maximum refinement levels can produce modification in the level of the inner entropy budget (up to a factor of 2 at the peak resolution investigated), the flat entropy core is present in all cluster resimulations (see also the additional resolution tests in the Appendix). This again calls for a mechanism of *physical* nature, which drives an efficient spreading of entropy enriched gas in the innermost regions of evolved clusters; this will be investigated in detail in the next Section.

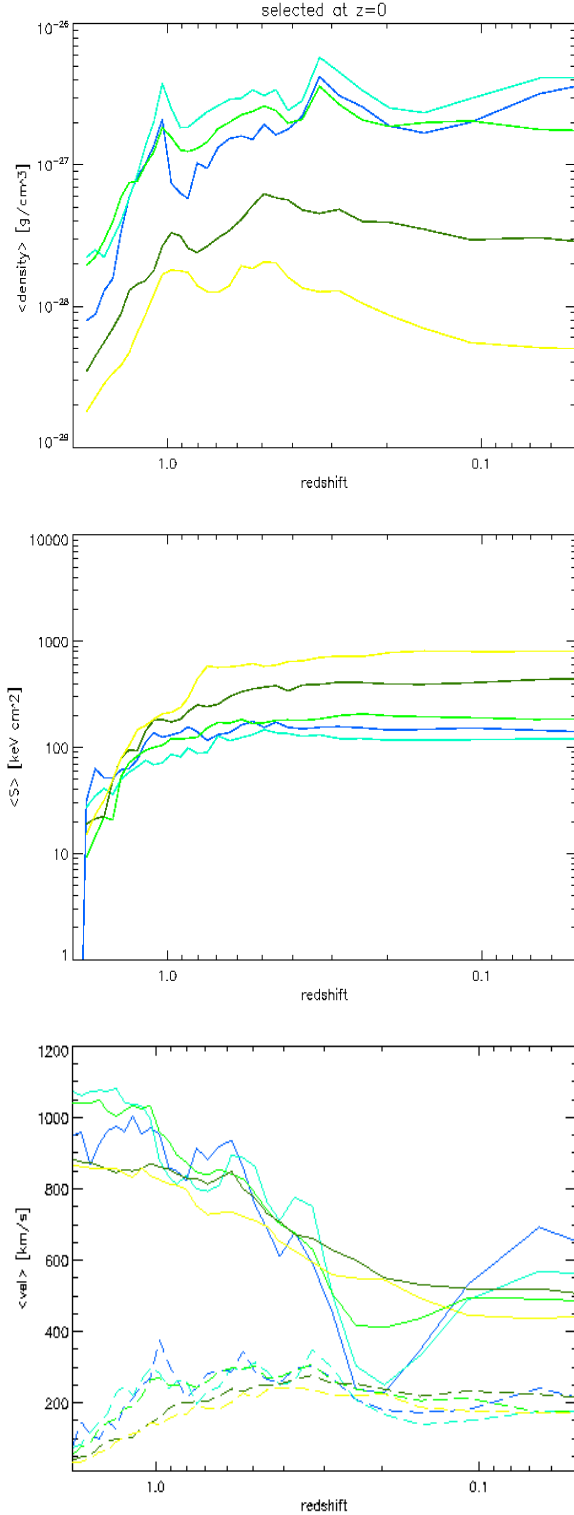


**Figure 11.** Time evolution of gas density (top panel), gas entropy (central panel) and mean gas velocity (or mean gas turbulent velocity, dashed lines) for the 5 groups of tracers selected according to their position in the cluster atmosphere at  $z = 0$ , as in Fig.10 (see Sec.4 for details).

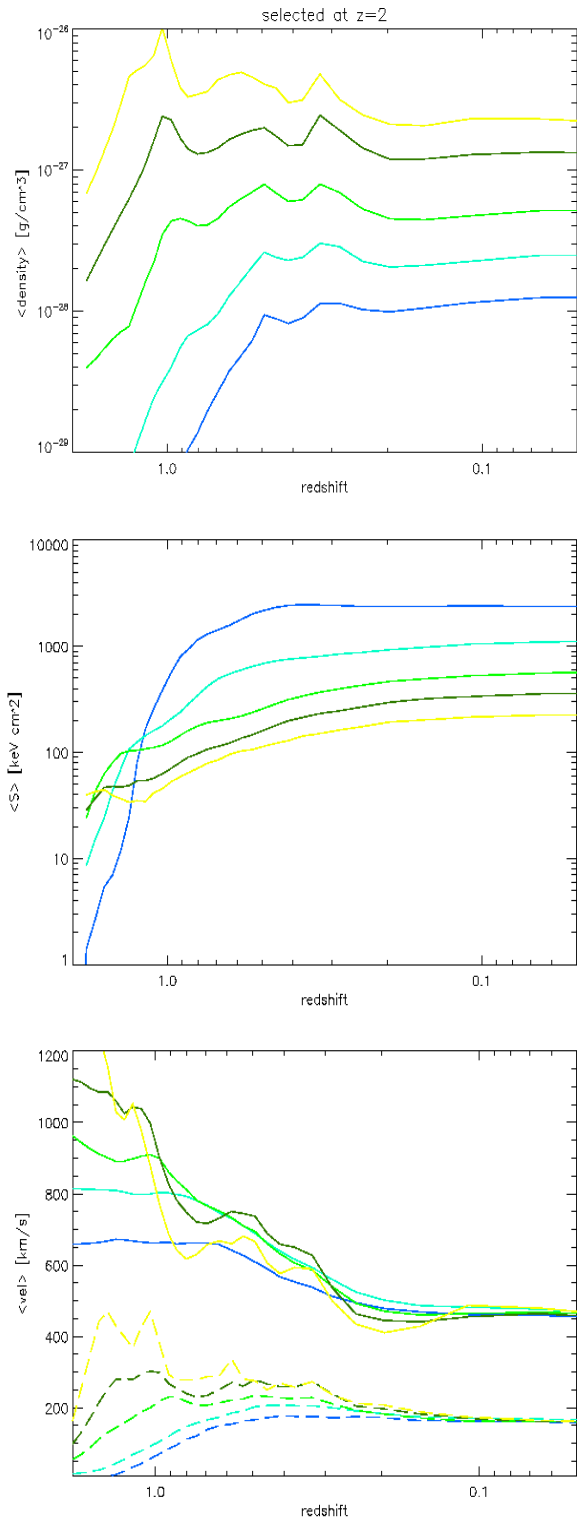


**Figure 12.** Time evolution of gas density (top panel), gas entropy (central panel) and mean gas velocity (or mean gas turbulent velocity, dashed lines) for the 5 groups of tracers selected at  $z = 2$  according to their initial gas density (see Sec.4 for details).

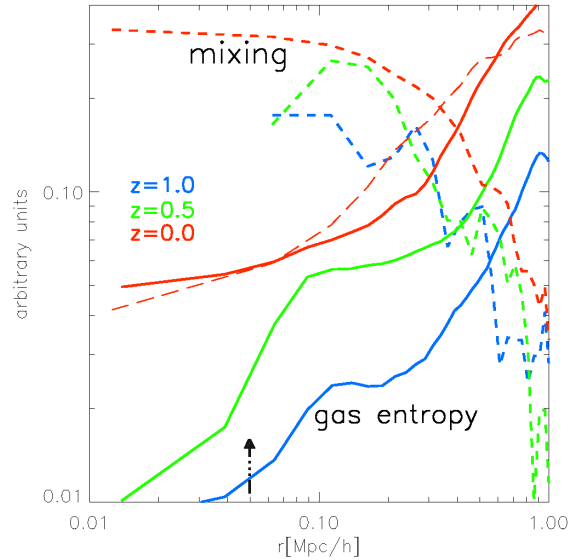


**Figure 13.** Radial profile of the mixing parameters for the tracers in run R0 (dashed lines) and radial profile of gas entropy (solid lines), at  $z = 1$  (blue),  $z = 0.5$  (green) and  $z = 0$  (red). The long-dashed line shows the radial profile of  $0.5 - M$  at  $z = 0$ . The gas entropy has been divided by 2000 for a better visualization. The vertical arrow show the softening length adopted in this run.

#### 4 PHYSICAL EFFECTS ON THE ENTROPY PRODUCTION.

The numerical tests reported in the previous Sections have shown that the presence of a regular low gas entropy distribution in galaxy clusters simulated with grid-based techniques is not a numerical artifact, rather but a very stable feature against a number of important changes in the possible setup of a cosmological simulation at high resolution.

At this point it is interesting to answer to the following questions: a) what is the main *physical* mechanism which sets the inner gas entropy distribution in a forming galaxy cluster, in non-radiative runs? b) Is the inner gas entropy distribution affected by a more sophisticated physical modeling of cluster dynamics (e.g. employing radiative cooling)? c) What is the effect of other non-gravitational extra-heating mechanisms (e.g. AGN feedback) on the the gas entropy profile of clusters?

In the following Section we explore how entropy is build over time in the same galaxy cluster analyzed above, by means of a Lagrangian approach based on tracer particles. In the other Sections, we analyze how is the entropy floor modified when a more realistic modeling of cluster physics is considered (e.g. assuming radiative cooling) and if extra-heating processes (e.g. uniform pre-heating or AGN feedback) are capable to reproduce an entropy distribution similar to that of the fiducial run.

##### 4.1 Where and when entropy is build in a forming cluster.

Passive tracers are a useful tool to follow the average trajectory of accreted baryons in a growing galaxy clusters, and to study the mixing pattern driven by accretion phenomena in clusters (Vazza, Gheller & Brunetti 2010). Here we use tracer particles to track the exact origin in time and space of the gas entropy deposited in the

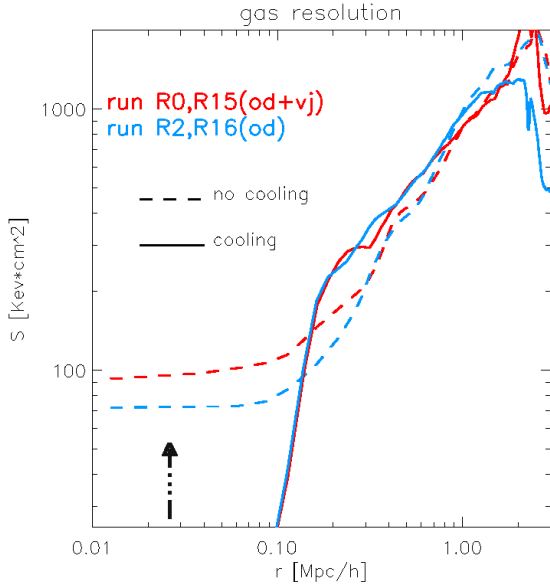


**Figure 14.** Comparison of the entropy profiles of radiative runs, using the standard mesh refinement (blue) and the velocity-based refinement (red). The additional dashed lines show the profile of the corresponding non-radiative runs (R0 and R2). The vertical arrow shows the softening length adopted in run R15 and R16.

cluster core of run R0, and to explain the emergence of a flat entropy core. We inject passive (mass-less) tracers in the simulation and let them be passively advected in the ICM using the information of the 3-D velocity stored for each snapshot of the simulation, in a post-processing phase. Convergence tests on the interpolation technique to assign velocities to tracers, on the time and space sampling are discussed in detail in Vazza, Gheller & Brunetti (2010).

In this particular case, we injected  $N = 10^5$  tracers at  $z = 2$  in the fiducial run (R0), within a cubic volume of  $\approx (10 \text{ Mpc}/h)^3$  centered in the AMR region. At this time the total virial mass of the forming cluster is only 10 – 15 per cent of its final mass at  $z = 0$  (Fig.1) and only small proto-clusters are present within the AMR region.

Tracers are initially placed with a random sampling of the volume, and then their positions are updated with the time steps finely saved in time of the original simulation, using a Nearest Grid Cell interpolation scheme (e.g. Hockney & Eastwood 1981). At all time steps, the tracers record the thermodynamic values of the closest cell in the grid distribution, and the whole thermodynamic history along the trajectory of every tracers can be recovered for analysis.

In Figure 10 we show the radial distribution of tracers at  $z = 0$ , plotting on the vertical axis the entropy of the nearest cell at each location. As a comparison, we overplot the (density weighted and volume weighted) entropy profile of the cluster, to confirm that tracers sample the underlying Eulerian distribution in an accurate way. At  $z = 0$  we selected 5 shells of tracers with width  $25 \text{ kpc}/h$ , located at the radii of  $r < 50 \text{ kpc}/h$ ,  $r = 150 \text{ kpc}/h$ ,  $r = 300 \text{ kpc}/h$ ,  $r = 600 \text{ kpc}/h$  and  $r = 1200 \text{ kpc}/h$  (shown as different colors in Fig.10). This allowed us to study the mean evolutive history of the parcels of gas ending at the different level in the cluster entropy profile at the end of the simulation. In Fig.11 we show the behavior of the mean gas entropy, gas entropy and velocity (or chaotic velocity, as measured in Sec.3.2) modulus for the 5 different shells, as a function of evolving cosmic epoch. Except for

the first bin (which contains  $N = 20$  tracers) for all the other shells the number is of the order of  $\sim 200$  and thus the mean values are very robust.

The sharp spikes in gas density (top panel) trace the main merging episodes which involve the different “shells” of tracers. The cluster entropy profile at  $z = 0$  is manifestly produced by a uniform and regular in time mechanism of “sorting in entropy”, which affects every tracers at the moment of its entrance in the virial region of the forming cluster (middle panel). The level of gas entropy in the cluster core is set, on average, during intense shock heating at  $z \sim 1$  (which also corresponds to the epoch of the most net increase in cluster mass, as shown in Fig.1). On the other hand the gas tracers with a larger entropy ( $S \sim 1000 \text{ keV cm}^2$ ) at the final epoch are found to be intensely shock heated at more recent epochs,  $z \sim 0.6 - 0.8$ . This analysis show that on average they belong to smooth, low density gas environment at  $z = 2$ , and that they are subject to smaller bulk and chaotic velocity fields at the final epoch, since they do not belong to bound in-falling structures (lower panel).

A complementary test was run by directly selecting 5 families of tracers at  $z = 2$  and sorting them according to their initial gas overdensity; their evolution is followed in Fig.12. The “sorting in entropy” among tracers is even more evident with this setup: the average values of gas density and gas entropy for the different families never overlap for  $z < 1$ , meaning that the main variable which sets the final entropy of a gas parcel ending up into a massive galaxy cluster is its initial overdensity. Say it differently, the fact that a gas particle is in a overdense (clumpy) environment around the forming cluster, determines on average the time at which it gains the bulk of the final entropy (in its first impact on the volume of the cluster under virialization), and its final distance from the cluster center, through the mechanism of entropy sorting in the main cluster atmosphere. This is in excellent agreement with the spherical analytic models of clusters forming in a hierarchical scenario, that prescribes a raising entropy at increasing radius from the cluster center, following the progressive deposition of shells undergoing stronger and stronger shock heating during the hierarchical growth of a cluster, (e.g. Tozzi & Norman 2001; Cavaliere, Lapi & Fusco-Femiano 2009).

This simple scenario may of course be more complicated in the case of a major merger, which can mix the intra cluster medium in a more efficient way (e.g. Mc Carthy et al.2007; Poole et al.2008; Vazza, Gheller & Brunetti 2010; ZuHone 2010).

The above tests show where and when the entropy profile is produced during the cluster evolution, but do not necessary imply the emergence of a small inner region of size  $r_{core} \sim 0.1 R_{vir}$  where the stratification is broken and the gas sets to the constant value of  $S \sim 100 \text{ keV cm}^2$  observed in the previous runs. A viable mechanism naturally produced by the accretion of matter onto the cluster is mixing of the inner gas layers, in response to chaotic motions in the ICM. To better compute the degree of mixing between Lagrangian tracers after their injection at  $z = 2$ , using a formalism introduced in Vazza, Gheller & Brunetti (2010). We introduce the mixing parameter of an “s” family of tracers,  $M_s$ , respect to all existing “i” families, by computing:

$$M_s = 1 - \frac{|n_s - \sum_i n_i (i \neq s)|}{\sum_i n_i}, \quad (2)$$

where  $n_s$  is the number density of the “s” tracers within a cell (at the highest resolution level) and the sum refers to all the species of “i” tracers (included the “s” specie). This formula generalizes the more simple case of mixing between two species (e.g. Ritchie

& Thomas 2002) and has a simple interpretation: for a cell where  $n_1 \approx n_2 \approx n_3 \dots \approx n_s$  the different families are well mixed and we have  $M_s \rightarrow 1$ , while  $M_s \rightarrow 0$  implies no mixing within the cell.

The total mixing in each cell,  $M$ , is the volume average between all species,  $M_i = \sum_s M_s/N_s$ , where  $N_s$  is the number of families considered. To obtain better statistics, the cell considered to compute  $M_i$  have a size which is double than the maximum gas resolution ( $50kpc/h$ ).

We sorted the density of all tracers at  $z = 2$  and divided the sample in 5 bins, each with 2000 tracers; then we computed the number density of each “s” family of tracers within the cluster, and computed the mean mixing  $M_i$  at different redshifts (Fig.13), only for those cells containing at least 1 tracer.

The profile of the mean mixing presents a regular trend in time, with a inner core of mixing material which is build as the cluster accretes matter, until an almost flat profile (with mean mixing  $M_i \approx 0.3$ ) is found for  $r < 100kpc/h$  at  $z = 0$ . Outside of this radius,  $M_i$  has a sharp decline towards the virial radius of the cluster, where the mixing is very poor  $M_i < 0.05$ . We verified that also different initial choices for the setup of the tracers sampling (e.g. by adopting a different number of tracers, or a different number of species) do not affect the above trend in any significant way.

Fig.13 shows the evolution of the gas entropy profile (solid lines) and of the mean mixing profile (dashed lines) for three redshifts. Quite clearly, the formation of the central entropy floor happens together with the formation of the prominent mixing pattern in the center of the cluster (the similarity of the two profiles is better indicated by overplotting the radial profile of  $| - M_i |$  at  $z = 0$ , long dashed line), and the  $S(r) \propto r^{1.1-1.2}$  scaling expected from SPH simulations (Voit et al.2005, Fig.6) is broken starting from the same radius for which  $M_i$  sharply increases to its maximum in the center. In Vazza, Gheller & Brunetti (2010) we provided evidence that in general the building of cluster entropy and of prominent mixing patterns are correlated features also in major merger systems (where, however, large and transient plumes of efficient mixing can be found also at large cluster radii); also recent FLASH AMR simulations (Zu Hone 2010) has lead to similar conclusions, based on a parametric study of binary cluster mergers. Usually the innermost region of cosmological cluster runs is characterized by small scale subsonic motions (on scales  $< 500kpc/h$  and  $\sigma_v \sim 0.3 - 0.5c_s$ , where  $c_s$  is the gas sound speed) continuously excited by the crossing of gas/DM material accreted within the cluster (e.g. Norman & Bryan 1999; Dolag et al.2005; Iapichino & Niemeyer 2008; Vazza et al.2009). In the case of ENZO AMR simulations these motions are well characterized by a power law spectrum for nearly two orders of magnitude in spatial scales (Vazza et al.2009; Xu et al.2009; Vazza, Gheller & Brunetti 2010); also the tracers pair-dispersion statistics show a well defined power-law dependence on time ( $P(t) \sim t^{3/2}$ , where  $P(t)$  is the distance between couple of tracers initially located at a small distance) compatible with a fairly fast transport motions in the turbulent ICM (Vazza, Gheller & Brunetti 2010).

When combined together, all the above evidences lead to the consistent conclusion that the emergence of a flat entropy floor in clusters simulated with grid codes is mainly due to the integrated effect of (mostly subsonic) turbulent motions in the evolving ICM. These motions are quite effective in mixing parcels of gas, which have been initially sorted according to the “entropy sorting” mechanism described above, generally inside  $r < 0.1R_{vir}$  and for late  $z < 1$  redshift, when that the bulk of cluster mass has been assembled. The same mechanism also applies when the standard mesh re-

finement is adopted, provided that the turbulent energy in the cluster core is smaller (Fig.5) and that the mixing and the transport of gas particles is significantly smaller (e.g. Fig.17 in Vazza, Gheller & Brunetti 2010).

It is well known that grid codes are prone to numerical mixing (i.e. different gas phases are forced to combine into an average cell value when their separation is smaller then the minimum available cell size) while in SPH gas particles do not mix entropy by construction, unless ad-hoc diffusion term is considered in the SPH equation (e.g. Agertz et al.2007; Price 2008; Wadsley et al.2008; Merlin et al.2010). Numerical mixing must be considered as an additional source of mixing also fro the ENZO AMR resimulations presented here. However the ubiquitous finding of evident mixing motions on scales much larger than the cell size discussed above, combined with the evidence that the entropy floor presents a very small evolution with the grid resolution, for peak resolution  $\leq 25kpc/h$ , indicate that numerical mixing cannot be the main responsible for the production of the entropy floor. According to this interpretation, the entropy floor is thus a result of mixing of the baseline steep  $S(r) \sim r^{1.1}$  profile (produced by the progressive shock heating of infalling shells of matter) within the region where the turbulent energy is maximum within cluster,  $< 0.1R_{vir}$ , as a result of the continuous excitement of a hierarchy of chaotic motions in the ICM driven accretion after accretion.

This is true for an inviscid treatment of the ICM, while the presence of magnetic fields and plasma viscosity may alter this picture in a significant way (e.g. Parrish & Quataert 2008; Ruszkowski & Oh 2010 and references therein).

In the following Sections, we will explore more realistic modelization of the same cluster, where non-gravitational mechanisms of entropy *decrease*, such as radiative cooling, and entropy *increase*, such as heating from energy feedback by stars of active galactic nuclei, are computed in run time.

## 4.2 The role of radiative cooling and pre-heating mechanisms.

Radiative cooling in galaxy clusters have a dramatic impact in the thermodynamics of the ICM, if no heating mechanism other than shock heating is available to balance the cooling catastrophe, for those cluster regions in which the gas cooling time is  $\ll$  of the cluster age (e.g. Katz & White 1993). Figure 14 illustrates the radial profiles of gas density, gas temperature and gas entropy for the two re-simulations with radiative cooling (assuming a fully ionized H-He plasma with a constant metallicity of  $Z = 0.3Z_\odot$ ) and with standard mesh refinement (R15) or velocity-based refinement (R16). In both cases, a steeply decreasing entropy profile develops towards the center of the cluster for  $r < 100kpc/h$ , with very low entropy values,  $S \ll 1keVcm^2$  in the center, a massive gas condensation peaking at  $10^{-24}gr/cm^3$  and a temperature dip with  $T \ll 0.1keV$ , similar to the classic theoretical cooling flow scenario (e.g. Fabian 1994).

We note that these simulations do not consider any prescription for star formation from the dense and cold phase of the ICM, and therefore the central condensation produced by run R15, R16 (see the solid black line in the top panel of Fig.16) would be significantly reduced by modeling star formation in a self-consistent way (e.g. Pearce et al.2000; Yoshikawa, Jing & Suto 2000; Valdarnini 2002). However this would make the pure cooling runs and the other explored in the next Sections more computationally expensive. We thus preferred to defer to the future the study of this issue, and to use this simplified cooling model without star forma-

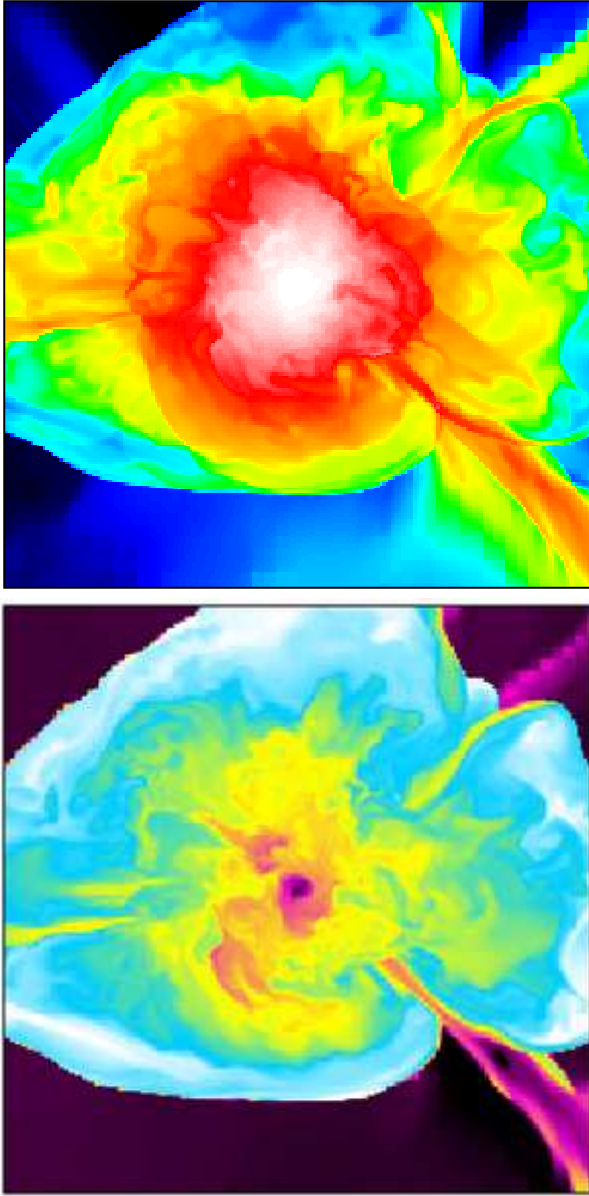


**Figure 15.** Maps of gas density (top panel) and gas entropy (bottom panel) for a slice taken in run B2 (cooling, pre-heating and refinement on velocity jumps). The side of the image and the meaning of colors are as in Fig.2.)

tion as the framework to study the effects of thermal energy feedbacks in the ICM, and the modification they cause to the gas entropy distribution.

In general major and moderate mergers (e.g. Burns et al.2008; Poole et al.2008) or gas sloshing triggered by the passage of DM/gas sub-clumps (e.g. Ascasibar & Markevitch 2006; ZuHone et al.2009) may significantly reduce the cooling catastrophe in radiative simulations, by exciting internal merger shocks or turbulent mixing in the clusters core. However, in the particular cluster simulated here the amount of chaotic motions excited for  $z < 1$  is never powerful enough to slow down the cooling flow in any significant way, even when the additional mesh refinement criterion is turned on. We report that also in the case of the merger system studied in the Appendix, the major merger at  $z \sim 0.85$  does not reduce the cooling catastrophe at the end of the simulation.

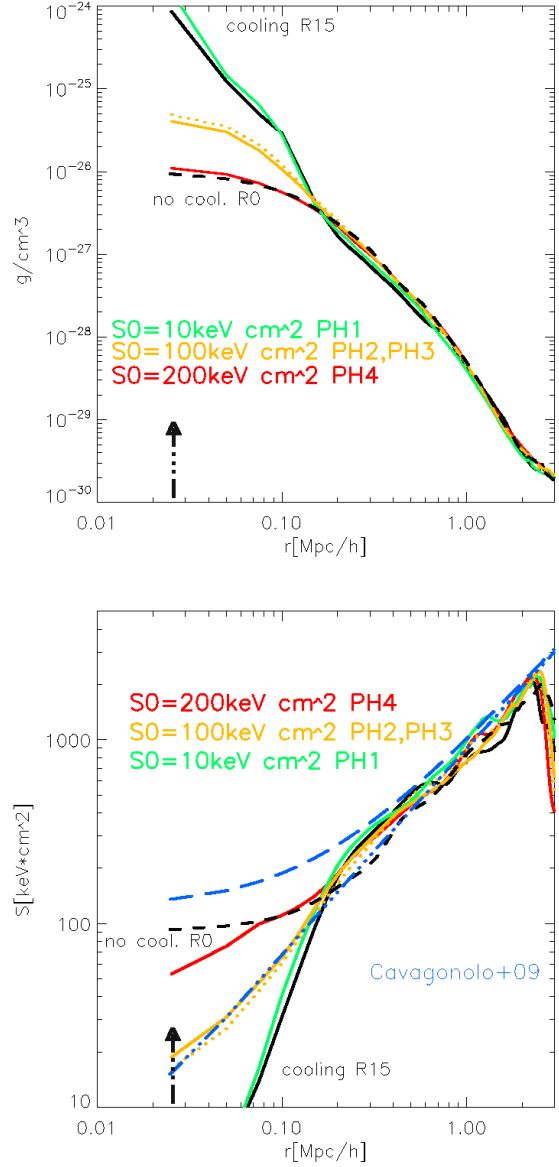


**Figure 16.** Gas density and entropy radial profiles for the run adopting pre-heating (run PH1  $S_0 = 10keV cm^2$ , run PH2  $S_0 = 100keV cm^2$  and run PH4  $S_0 = 200keV cm^2$ ). The dotted lines show the result for the run PH3, adopting  $S_0 = 100keV cm^2$  and standard mesh refinement. The additional black lines shows the profile for the non-radiative run (run R0, long dashed) and for the cooling run (run R15, solid). We also overplot in blue the best fit profiles of Cavagnolo et al.(2009), with a core entropy of  $S_0 = 15keV cm^2$  (dot-dashed) and  $S_0 = 150keV cm^2$  (long-dashed). The vertical arrow in both panel show the softening lenght adopted in the runs with cooling and pre-heating.

As widely known, cluster configurations according the "pure cooling" scenario are not observed in the real Universe, and the gas temperature in real clusters is never observed below  $\sim 0.1keV$  (e.g. Rossetti & Molendi 2010 and references therein). For this reason, additional sources of gas heating were considered in order to reconcile simulations with observations. In what follows, we will apply some of the most promising models of extra-heating developed in the literature to our cluster simulations, and study their impact on the gas entropy profile at  $z = 0$ .

#### 4.2.1 Early pre-heating.

Motivated by the early evidences of significant departures from self-similar scalings expectations in observed galaxy clusters (e.g. White 1991; Evrard & Henry 1991; Ponman, Cannon & Navarro 1999; Lloyd-Davies, Ponman & Cannon 2000), several authors proposed a "pre-heating" scenario, in which an energy input of non-gravitational origin is injected in the Intra Galactic Medium at early redshift ( $z \sim 3 - 10$ ). This smoothens the gas of in-falling primordial halos of low mass and supplying the innermost region of massive cluster of an amount of high entropy gas, to reconcile with observations. (e.g. White 1991; David, Forman & Jones 1991; Kaiser 1991; Evrard & Henry 1991; Cavaliere et al.1997; Voit et al.2005). This early heating may be provided by a number of sources, such as star formation and SNe explosion, radiative and mechanical heating from AGNs, radiative heating from hard X-ray background, etc (e.g. Tozzi & Norman 2001). The estimated needed amount of extra entropy at high redshifts falls in the range  $100 \leq \Delta S \leq 300 keV cm^2$ , and viable sources of it in the early Universe can be supernovae explosions, star formation and galactic winds. From the numerical viewpoint, several group attempted to model this process either by imposing an impulsive entropy injection at a given epoch (e.g. Bialek, Evrard & Mohr 2001; Borgani et al.2005; Kay et al.2007; Romeo et al.2006; Younger & Bryan 2007) or in a redshift-modulated way (e.g. Borgani et al.2002; Sijacki et a.2007; Mc Carthy et al.2009).

An important drawback of early pre-heating models could be that they tend to remove too much low entropy gas from lower mass halos, without obtaining a realistic galaxy population (e.g. Donahue et al.2006). In addition, recent results based on XMM-Newton analysis presented by Rossetti & Molendi (2010) proved that most of non-cool core clusters host regions with low entropy and high metallicity, suggesting the possibility of a recent transition between cool core and non-cool core systems, contrary to the pre-heating scenario (e.g. Guo & Mathews 2010).

As a first step to investigate the role played by non-gravitational heating on the entropy level of our cluster, we tested early pre-heating models following the prescription of Younger & Bryan (2007).

The thermal energy within each gas cell in our cluster run is selectively increased at  $z = 10$  by:

$$k_B \Delta T = S_0 \left[ \frac{\rho}{\mu m_p} \right]^{\gamma-1}. \quad (3)$$

In detail we re-simulated run R15 (velocity based refinement and cooling) by imposing the entropy floor of  $S_0 = 10 keV cm^2$  (run PH1),  $S_0 = 100 keV cm^2$  (run PH2) and  $S_0 = 200 keV cm^2$  (run PH4). Smoothing the gas density distribution of halos at high redshift is expected to affect the shock heating process in forming structures, through "entropy amplification" at strong accretion shocks (Voit et al.2005). To highlight the dependence of this mechanism on the accuracy with which accretion shocks are modeled in our runs, we also tested the intermediate pre-heating scenario of run PH2 ( $S_0 = 100 keV cm^2$ ) in the standard mesh refinement strategy alone (run PH3).

Figure 15 shows the effect of pre-heating in extreme case of run PH4 at  $z = 0$ . Compared to the non pre-heated scenario (run R0) the global cluster morphology is smoother, and the accretion pattern are more regular in shape, since most of the accreted gas clumps were smoothed by the early heating episode. In Fig.16 we compare the gas density and gas entropy profiles for the runs employing pre-heating, against the profiles of the fiducial run (R0) and of the simple cooling run (run R12).

Consistently with the literature, we find that energy inputs corresponding to  $S_0 = 100 - 200 keV cm^2$  are capable of keeping the in-falling gas on an higher adiabat, preventing the core gas to cool below  $\sim 0.5 keV$ . In particular, the pre-heating prescription of run PH4 is suitable to recover the gas density and the gas entropy of the non-radiative run (R0), within a  $\sim 10 - 20$  per cent at all radii. A similar result is also found for the major merger system studied in the Appendix. On the other hand, the uniform pre-heating model with  $S_0 = 10 keV cm^2$  is found to be insufficient to prevent the cooling catastrophe and the resulting cluster profile is almost identical to that of run R15.

The trend found is qualitatively in agreement with the results of Borgani et al.(2005) and Younger & Bryan (2007), even if our study is based on a single object and no conclusion about the most suitable values of  $S_0$  needed to reconcile with observations can be derived in a statistical sense. We also note that the final entropy configurations of run PH2, PH3 and PH4 are compatible with the bimodal distributions of entropy profiles of obtained with CHANDRA (Cavagnolo et al.2009, additional blue lines in Fig.16). This work recently suggested the existence of two broad population of clusters, characterized by an inner entropy value of  $S \sim 15 keV cm^2$  or  $S \sim 100 - 150 keV cm^2$ , and a large radial behavior scaling as  $S(r) \propto r^{1.1}$ . Our cluster is a relaxed one at  $z = 0$ , and the fact that it is more similar to the "low entropy core" class of CHANDRA clusters, even when  $S_0 = 200 keV cm^2$  is applied, is fully compatible with the idea that "high entropy core" class is produced only by those clusters with a sufficiently violent merger in their past (e.g. Rossetti & Molendi 2010).

#### 4.2.2 Heating from AGN jets.

The most successful models to achieve a balance with radiative cooling during the simulated evolution of clusters rely on heating by outflows from an AGN hosted by the central massive galaxy (e.g. Churazov et al.2000; Bruggen & Kaiser 2002; Brighenti & Mathews 2003; Dalla Vecchia et al.2004; Zanni et al.2005; Heinz et al.2006).

The self-consistent modeling of AGN heating in evolving galaxy clusters, in connection with the matter accretion history of the central massive cD galaxy has become only quite recently within the capability of full cosmological simulations (e.g. Sijacki & Springel 2006; Dubois et al.2010). In general, this issue is made complex by the (still unclear) role played by other physical mechanisms relevant to the thermodynamic evolution of the cluster plasma: plasma viscosity, magnetic fields, Cosmic Rays, etc (e.g. Bruggen & Kaiser 2001; De Young 2003; Brighenti & Mathews 2003; Ruskowski et al.2007; Sijacki et al.2008; Xu et al.2008; O'Neill & Jones 2010; Scannapieco & Bruggen 2010).

In this Section, we study the energy budget necessary to quench the cooling catastrophe developed in our radiative run (R15), using the *thermal* feedback from an assumed central AGN (e.g. Booth & Schaye 2009; Teyssier et al.2010) This is done by injecting localized inputs of extra-thermal energy, starting at  $z = 1$  in run R15, in the region of the cluster density peak, where the AGN is assumed.

This is motivated to mimic the thermal feedback response from a central AGN which releases as feedback a fraction of the rest mass energy of the accreted cold gas, with an efficiency which is generally assumed to be in the range of  $\sim 0.01 - 0.1$  of the total energy radiated by the super massive black hole (e.g. Booth & Schaye 2009; Giodini et al.2010 and references therein). In our setup, we assume that the feedback manifests itself at the scale of

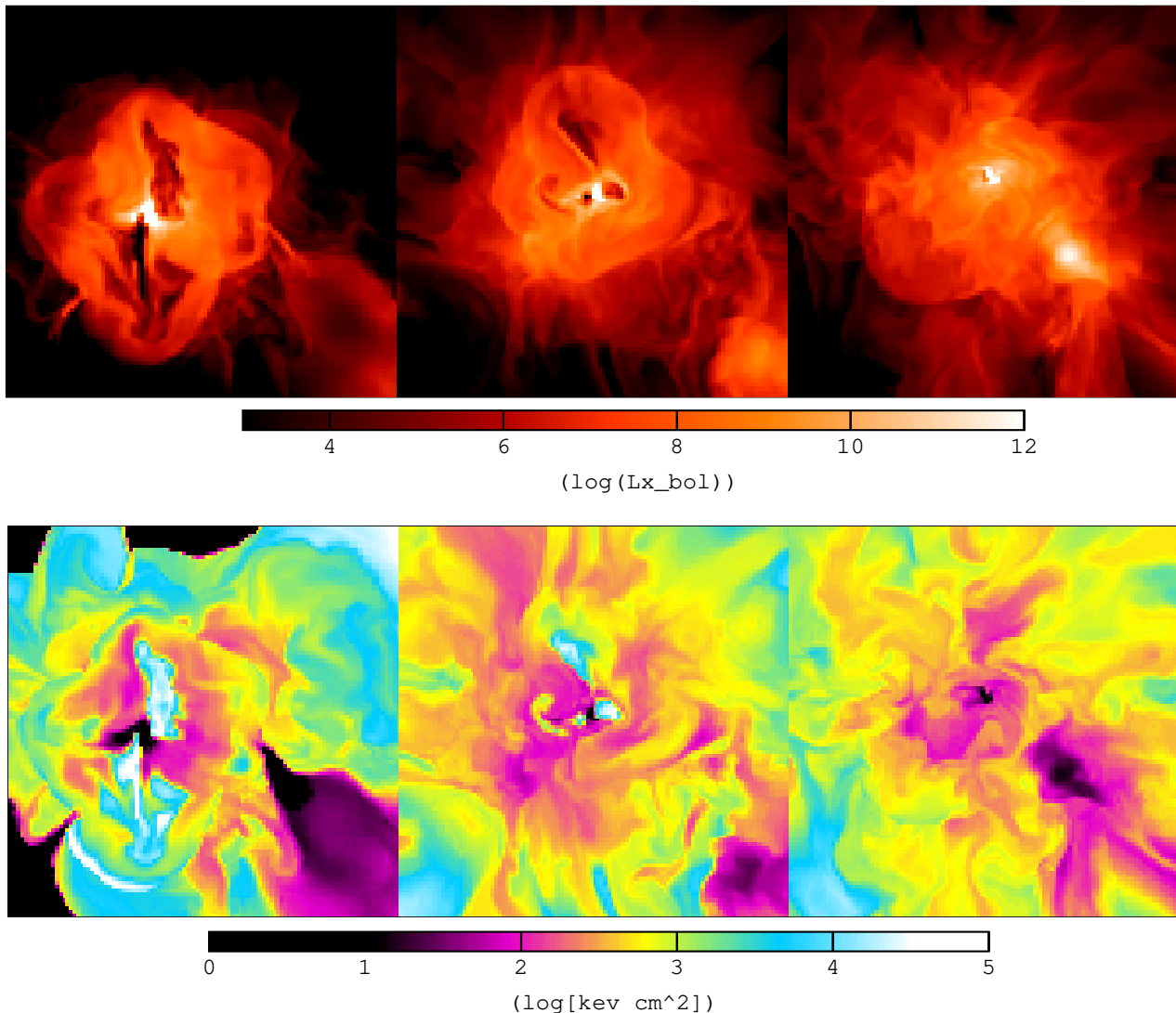


**Figure 17.** Cuts through the center of the simulated cluster, showing the evolution of the bolometric x-ray luminosity (top panels, arbitrary units) and gas entropy (bottom panels) for run B2. From the left to right, the epoch shown are  $z = 0.96$ ,  $z = 0.85$  and  $z = 0.75$ . The side of the images is  $2.7 Mpc/h$ .

the maximum gas resolution in the cluster center ( $25 kpc/h$ ), as the injection of two point-like over-pressurized “bubbles”, produced by the interaction between the launched jets and the surrounding cold ICM. The thermal energy at the location of the “bubbles” is updated as:

$$E_{thermal} = \frac{3k_B \rho T \Delta x^3}{2\mu m_p} + \frac{\epsilon'_{jet}}{2} \quad (4)$$

where  $\mu$  is the mean molecular mass,  $m_p$  is the proton mass, where  $\Delta x^3$  is the volume of the cell, and  $\epsilon'_{jet}$  is the fraction of  $\epsilon_{jet}$  released at every injection episode. The 3-D velocity field at the injected bubbles is left unchanged. Therefore in our treatment  $\epsilon'_{jet}$  represents the thermal energy released in the ICM by the two jets at a given time step, after the thermalisation of a part of their mechanical energy, which is assumed to happen on a sub-grid scale. The “bubbles” are initially located at the distance of  $d_{jet} = 50 kpc/h$ , at two opposite sides of the gas density peak of the cluster, starting from  $z = 1$  in run R15 (or run R16 for the standard refinement strategy). The injection is performed before the

hydro step of the PPM scheme, by updating the gas internal energy following Eq.4 of two cells (at the maximum resolution level) according to 4; then the Riemann solver in ENZO is evolved in the usual way.

Preliminary tests showed that the impulsive injection of the whole  $\epsilon_{jet}$  in a single time step of the simulation produces unrealistically strong (e.g.  $M > 10$ ) shock waves in the cold and dense cooling flow cluster region. Since only mild shocks are observed in jets/bubbles interaction with the ICM of real clusters (e.g. Simionescu et al.2009; Werner et al.2010), we preferred to adopt a more gradual release of energy from the central gas peak, by distributing  $\epsilon_{jet}$  in  $\sim 20$  injection episodes, across a total time of  $\sim 3 Gyr$ , preserving the same orientation for the “jets” axis. In principle, idealized but more self-consistent recipes to link the feedback energy with the matter accretion rate within the cooling region can be applied to cosmological simulations (e.g. Sijacki & Springel 2007; Booth & Schaye 2009); however here we want to investigate how different re-simulations of the same object react to a *constant* model of extra thermal energy release from a cen-



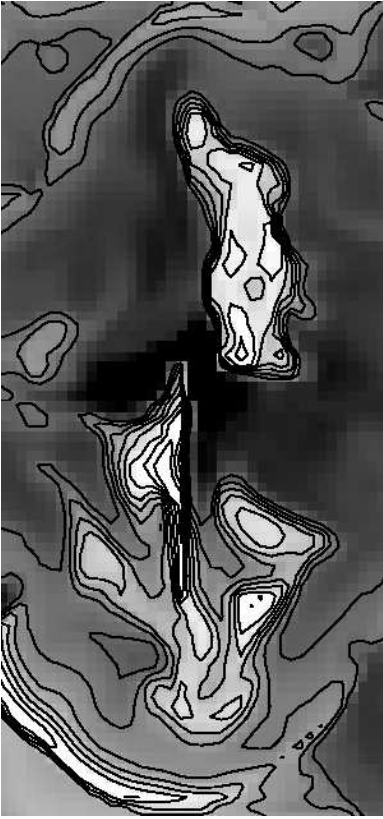


**Figure 18.** Zoomed view of the internal ICM region after the first AGN outflows in run B2 at  $z = 0.96$  (logarithmic view of gas entropy). The isocontours are drawn only for gas with  $S > 500 \text{ keV cm}^2$  to highlight the contribution from the AGN burst. The scale of the images is  $\sim 1.5 \times 0.5 \text{ Mpc/h}$ .

tral AGN. We defer to the future any study of more self-consistent setup of the feedback energy, and of the way it is released within the ICM (e.g. by varying the jets orientations in time, by assuming an "quasar mode" and "radio mode" feedback, etc).

With our setup, only  $M < 5$  shocks are produced, even in the most extreme scenario investigated, and only in the starting phase of the jet, when the surrounding ICM is in its coldest phase. Our trials adopted  $\epsilon_{jet} = 10^{58} \text{ erg}$  (run B1) and  $\epsilon_{jet} = 10^{59} \text{ erg}$  (run B2); this makes the typical power of our jets in injection phase of about  $W_{jet} \sim \epsilon'_{jet}/t_{step} \sim 10^{42} - 10^{43} \text{ erg/s}$  ( $t_{step}$  is  $\sim 4 \cdot 10^7 \text{ yr}$  at that epoch). We note that the power for the energy release of our jets in the surrounding medium, and the assumed duty cycle and duration are within most of the estimated energy budget provided by the observations of AGN activity reported by many authors (e.g. Birzan et al.2004; Dunn & Fabian 2006; Wise et al.2007; Giacintucci et al.2008; Bird, Martini & Kaiser 2008; Worrall et al.2009; Liuzzo et al.2009; Sanders & Fabian 2009; Gu, Cao & Jiang 2009; Gitti et al.2010; Giodini et al.2010).

Scannapieco & Bruggen (2008) have recently shown that a proper treatment of turbulence on  $< 10 \text{ kpc}$  scales is mandatory to model the full interaction between jet-inflated bubbles and the ICM, because this may change the rate of energy transfer to the surrounding cold phase of the ICM. Therefore, it is unlikely that our simulations are fully converged, and further tests at higher resolution will be needed in the cosmological framework. In any case, we assess the role played by numerical resolution here by running two additional re-simulations, using only standard mesh refinement, (run

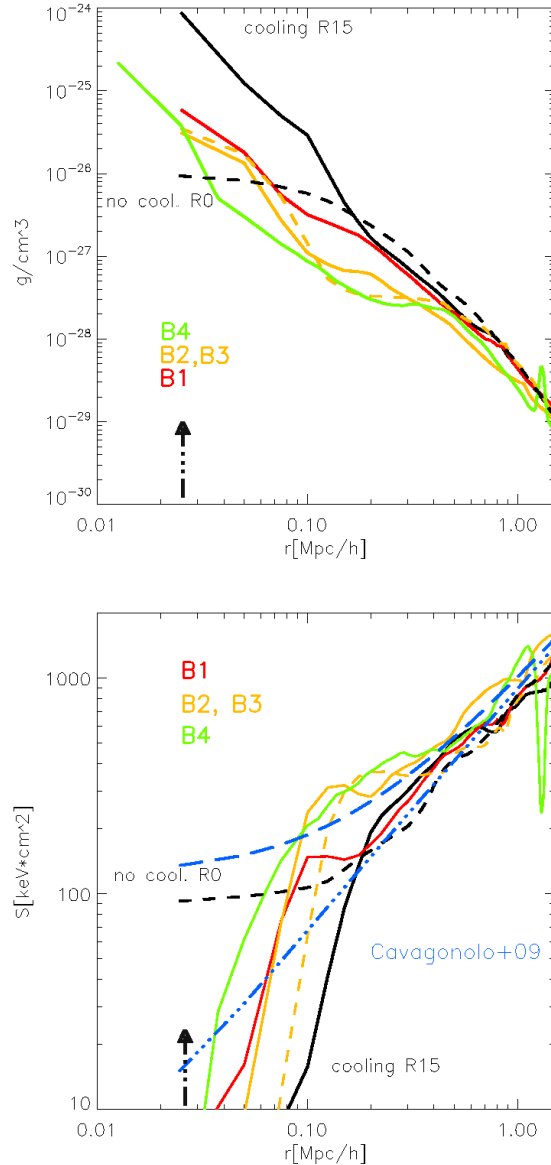


**Figure 19.** Gas density and entropy radial profiles for the run adopting AGN jets feedback (run B1, B4  $\epsilon_{jet} = 10^{58} \text{ ergs}$ , runs B2  $\epsilon_{jet} = 10^{59} \text{ ergs}$ ). The dashed lines show the result for the run B3, adopting  $\epsilon_{jet} = 10^{59} \text{ ergs}$  and standard mesh refinement. The additional black lines shows the profile for the non-radiative run (run R0, long dashed) and for the cooling run (run R15, solid). We also overplot in blue the best fit profiles of Cavagnolo et al.(2009), with a core entropy of  $S_0 = 15 \text{ keV cm}^2$  (dot-dashed) and  $S_0 = 150 \text{ keV cm}^2$  (long-dashed). The additional arrow in both panel shows the softening length adopted in the runs with cooling and AGN feedback.

B3) and using an additional level of refinement in the velocity based strategy, up to a maximum resolution of  $\Delta x = 12.5 \text{ kpc/h}$  (run B4).

The evolution of bolometric X-ray luminosity and gas entropy in a slice crossing the cluster center for run B2 is shown in Fig.17. Soon after the first injection, two vertical outflows has developed for  $\sim 400 - 500 \text{ kpc}$  along the axis of "bubbles" injection and has pushed the dense and low entropy material out to larger radii. The first feedback episode drives a mild shock in the cold ICM, with

$M \sim 3.5$ , while along the outflows Kelvin-Helmholtz instabilities develop and favors the mixing between the cold uplifted gas from the core and the surrounding hotter ICM (Fig.4.2.1). The outflows that follow inflate more stable "bubbles" (central panel in Fig.17), which are initially less overpressurized compared to the surrounding ICM, heated by the previous feedback episode. These bubbles only drive weak  $M \sim 2$  shocks around the central gas condensation. In addition, the sloshing motions in the cluster center are powerful enough to bend the initial orientation for the bubble launching, and to partially provide azimuthal mixing of the injected entropy.

Compared to the fiducial run (R0) or to the pre-heated runs (PH2,PH4), we found that the large scale accretion patterns are modified by the outgoing propagating shocks that follow the AGN activity.

In Figure 19 we compare the the gas density and gas entropy profiles for all trials at  $z = 0$ . We found impossible to recover an entropy profile similar of the fiducial run (and also with the results of Cavagnolo et al.2009, overplotted in the same Figure): the extra energy of shocks is very efficiently delivered to larger cluster radii by the shocks, which develop in the interaction between the cooling ICM and the hot bubbles phase. As a result, in these configurations we find an excess of gas entropy for  $r > 75kpc/h$ , compared to the radiative and non-radiative cases and a flat entropy profile inside the cluster core. However these runs produce a much smaller cooling region ( $r_{cool} < 50kpc/h$ ) compared to the  $r_{cool} \approx 100kpc/h$  of pure cooling models (run R15, R16). The observed steepening of the internal gas entropy after the AGN energy released is in good agreement with the semi-analytical prediction of a quasar-driven blasts in clusters discussed in Lapi, Cavaliere & Menci (2005), further suggesting that in the trials investigated here the shock heating mechanism is the main mechanism which interchanges energy between the AGN and the surrounding ICM.

When the mesh refinement is triggered uniquely by gas/DM over-density (run B3), the final entropy profile at  $z = 0$  present a larger cooling region (in-between the pure cooling case and the B2 re-simulation). In this case it is difficult to disentangle the effect of the under-sampling issues of satellites-driven mixing (Sec.4.1) from that of the under-sampling of jet-driven turbulence around the cluster core. The re-simulation with an additional level of mesh refinement (run B4) shows that as resolution is increased the final size of the cooling region is reduced, and the entropy at larger radii is increased, due to a better modeling of shocks induced by the outflows and of the driven turbulent motions. Further studies will be needed in the future to fix the best resolution needed for full numerical convergence in these features.

Our general conclusion is that, even if the action of feedback from outflows in our simplified implementation efficiently reduces the size of the cooling flow region compared to a pure radiative run, it remains difficult to reproduce a flat inner entropy profile as in the non-radiative case. The problems is not in the energy budget assumed in the outflow (which is a reasonable energy budget available to observed AGNs) but rather in the mechanism which transfers to the surrounding medium, which is mainly shock heating of the cold central ICM (see also Zanni et al.2004; Lapi, Menci & Cavaliere 2005). It is likely that more gentle mechanisms of feedback from the central AGN, such as a more gradual deposition of many by inflated bubbles(e.g. Churazov et al.2001; Bruggen et al.2007), can be more efficient in stopping the catastrophic cooling in our run. However in that case a significantly larger resolution than the one available here must be considered, which is presently difficult for AMR runs with our mesh refinement scheme. In addition, sub-grid modeling of turbulence may necessary (e.g. Scannapieco & Bruggen 2010) and also physical energy component,

such as magnetic field and relativistic particles, should be important to attach this problem (e.g. Bruggen & Kaiser 2001; De Young 2003; Brighenti & Mathews 2003; Ruskowski et al.2007; Sijacki et al.2008; Xu et al.2008; O'Neill & Jones 2010; Scannapieco & Bruggen 2010; De Young 2010).

#### 4.2.3 Hybrid external and internal extra-heating models.

Early ( $z \sim 3 - 10$ ) pre-heating and late ( $z < 2$ ) AGN feedback models account for a variety of energy exchanges between active galaxies and the diffuse baryon gas finally forming a galaxy cluster. The main physical difference between the two regimes is that pre-heating acts as an *external* heating mechanism, modifying the entropy of baryons in a pre-collapse phase, while AGN feedback is an *internal* heating mechanism acting within the already formed DM potential well of a massive halo. The two scenarios imply a very different energetic budget, since for the same given entropy level a larger energy per particle is required at higher cosmic density (e.g. Tozzi & Norman 2001; Mc Carthy et al.2008). Only quite recently cosmological numerical simulations have achieved sufficient resolution and complexity to follow the interplays between the ICM and the populations of galaxies in a self-consistent way, along the whole cosmic evolution (e.g. Sijacki et al.2008; Teyssier et al.2010; Dubois et al.2010; Mc Carthy et al.2009).

In order to match the two approaches in the same cluster run, we investigated a re-simulation adopting the intermediate ( $S_0 = 100keVcm^2$ , run PH2) scenario for early pre-heating, and less powerful jets at  $z = 1$ , with  $\epsilon_{jet} \approx 2 \cdot 10^{57} ergs$  (run B5).

In Fig.20 we show how the inner gas density and gas entropy of run PH2 (top panel) are modified by the late jets activity (bottom panel): a vertical structure of gas with entropy  $S \sim 100keVcm^2$  is found at the opposite sides of the cluster center, resulting in significant entrainment of the cold and dense gas of the cluster core, which is uplifted to larger radii at  $z = 0$ . In consequence of this, the inner density core is significantly depleted compared to run PH2 at the same redshift.

In Fig.21 we compare the profiles of gas density and gas temperature for the non-radiative run (R0, dashed black line), of the radiative run with strong pre-heating (run PH4, in red) and of run B5 (blue). Since the moderate amount of early pre-heating already prevented over-cooling of the gas in the cluster core for  $z > 1$ , the late injection of jets do not drive of shocks stronger than  $M > 2$ , and the extra entropy input is more uniformly released within the cluster core through mixing, rather than through violent shock heating. Indeed, the gas entropy profile and gas density profile are very similar to the non-radiative case (run R0, solid blue line), and a well defined entropy floor is recovered; the similarity is even more evident at  $z = 0.3$  (dashed blue line),  $\sim 2Gyr$  after the end of the jet injection.

We conclude that, when the thermal properties of the cluster are concerned, the same configuration produced in a non-radiative run can be approximately achieved also in a radiative simulation, thanks to the combined effect of a uniform *external* pre-heating of  $S_0 \sim 100keVcm^2$  at high ( $z \sim 10$ ) redshift and of a later phase of *internal* heating from jets injected by AGN at  $z \sim 1$ , characterized by an average power of  $W_{jet} \sim 2 \cdot 10^{41} erg/s$ .

This is in line with results obtained with semi-analytical 1-D calculation presented in Mc Carthy et al.(2008), and illustrates one of the (likely many) possible combinations of external and internal heating mechanisms and radiative cooling in realistic galaxy cluster simulations. Of course this result is derived only from a sin-

gle cluster object only, and additional re-simulations considering a wide range of masses and dynamical state are necessary to investigate the above issues even in a statistical sense.

We note however that the kinematic structures of the ICM velocity field in the various run are very different (Fig.22): the non-radiative run R0 is characterized by a peaked velocity profile, with an infall velocity of  $\sim -200\text{km/s}$  within the cluster core, due to the presence of a crossing satellite. On the other hand the other runs with additional heating and cooling do not present this feature; this is due to the fact that the same gas clump have been destroyed in the past by the action of early-preheating and enhanced shock heating while crossing the main cluster virial radius. In addition, the run with moderate jet feedback (run B5) shows a sharp velocity structure in the profile of radial velocity with  $+250\text{km/s}$  at  $\sim 200 - 400\text{kpc/h}$ , and a quite flat inner velocity profile, after the forcing of AGN outflows in the past. We note that similar features in the radial velocity field, in response to AGN feedback, have been recently reported by Dubois et al.(2010) for cosmological simulations with the RAMSES code.

This kinematic differences should lead to different large scale patten of mixing/metallicity, and could be used to discriminate among degenerate thermodynamical structures of galaxy clusters, to be compared with real observations provided by future high resolution spectroscopic observations of the ICM.

## 5 DISCUSSION AND CONCLUSION

In this paper we presented a detailed numerical study on the numerical and physical reasons for the presence of a flat entropy core in the innermost region of galaxy clusters, simulated in cosmological grid simulations adopting AMR (with customized version of the code ENZO). To this end, we performed 30 cosmological re-simulations of the same non-major merger cluster of final mass  $M \approx 3.1 \cdot 10^{14} M_{\odot}/h$ . We accurately studied the many parameters likely affecting the production of physical or numerical entropy within cosmological cluster simulations.

Evidences were presented for the *ubiquitous* presence of a well defined entropy floor inside the cluster core radius of non-radiative cosmological runs, mostly independently on the numerical details of the simulations (Sec.3). This plateau-like entropy distribution ranges from  $\sim 70\text{keV} \cdot \text{cm}^2$  to  $\sim 150\text{keV} \cdot \text{cm}^2$ , and has a size of  $r_{\text{core}} \sim 100 - 200\text{kpc/h}$  ( $\sim 0.1R_{\text{vir}}$ ) at  $z = 0$ . The most relevant factor affecting the level of entropy in the cluster core, among those investigated, is the mesh refinement strategy adopted in the simulation (Sec.3.2): when mesh refinement triggered by velocity jumps is added to the standard mesh refinement triggered by gas/DM over-density, the level of entropy in the core is increased by a factor  $\sim 1.5 - 2$ . This is due to the enhanced presence of mixing motions and shocks within the cluster, which are otherwise more dampened by under-sampling effects in a standard refinement strategy. The other effects (N-body gravitational noise, cold unresolved flows, softening length in the calculation of DM dynamics, spatial resolution for gas dynamics) were found to introduce differences at the order of a few tens of percent on the final entropy profile, without changing the inner slope of the radial distribution in a relevant way (Sec.3.3-Sec.3.5).

In Sec.4.1 we explored in detail the physical mechanism which produces the flat entropy distribution in non radiative cosmological simulations, using Lagrangian tracers advected in the simulation. The regular accretion of shells of matter onto the forming cluster is responsible for the strong entropy stratification found for

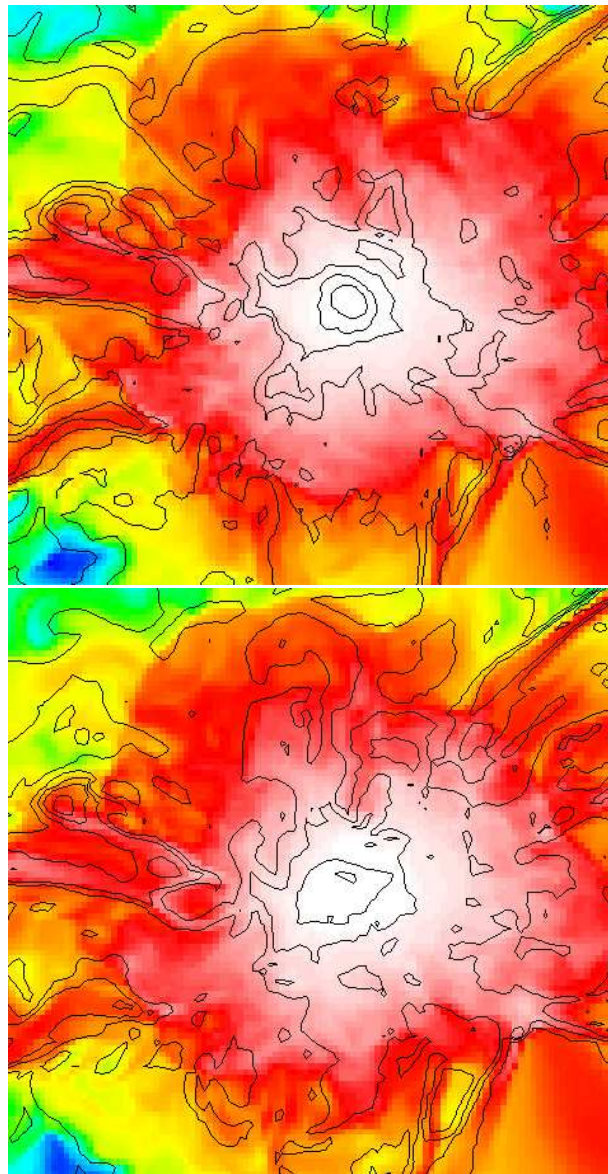


**Figure 20.** Gas density (colors) and gas entropy (contours spaced in  $\Delta \log(S) = 0.2$ ) for central region of run PH2 (top panel) and run B5 (bottom panel). The side of the images is  $2.5\text{Mpc/h}$ ; the colors are as in Fig.2.

$r > 100\text{kpc/h}$  at the final epoch; this stratification sets up already in the first phases of the collapse ( $z \sim 1-2$ ), and mirrors the different thermodynamic history of clumpy and smooth accretions onto the main cluster. Inside  $r < 100\text{kpc/h}$ , mixing motions driven by matter accretion gradually mix lower and higher entropy gas, producing an almost constant entropy profile in the region where the gas+DM gravitational potential is shallow. Our results here confirm and extend the seminal work of Mitchell et al.(2008) to a fully cosmological framework, and to non-major merger galaxy clusters.

We also explored more complex physical modeling of the ICM, following the effect of radiative cooling (Sec.4.2) and of non-gravitational heating mechanisms, such as early uniform pre-heating (Sec.4.2.1) or late jets-like injection by AGN (Sec.4.2.2). We report that, while it is feasible to recover a very similar profile of non-radiative runs and of observed CHANDRA clusters (Cavagnolo et al.2009) with a suitable choice of uniform extra-entropy

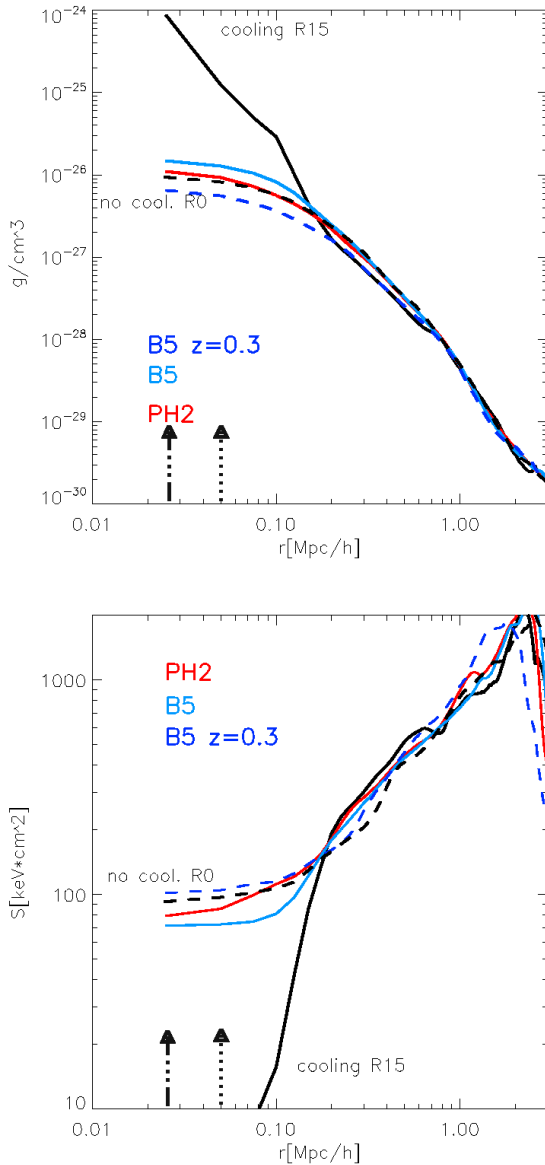


**Figure 21.** Gas density and entropy radial profiles for the run PH2 (red), run B5 at  $z = 0$  (solid blue) and  $z = 0.3$  (dashed blue). The additional black lines shows the profile for the non-radiative run (run R0, long dashed) and for the cooling run (run R15, solid). The vertical dotted arrow shows the softening length adopted in run R0, while the dot-dashed one shows the softening of runs PH4 and B5.

input at  $z \sim 10$  (in the range of  $S_0 \sim 100 - 200 \text{ keV cm}^2$ ), it results impossible to achieve similar results with the set of trials of only jet-like injections, where we simulated the thermal feedback from a central AGN. In the explored configuration, the main problem is that the bulk of the energy release from AGN outflows triggers too intense shock heating in the cooling ICM at  $z \sim 1$ , and *steepens* the inner gas entropy profile as shown in semi-analytical model presented in Lapi, Cavaliere & Menci (2005). However, the adoption of a hybrid model with moderate early pre-heating and late and modest jets feedback (Sec.4.2.3) is found suitable to recover a thermodynamic structure which extremely similar to the non-radiative fiducial run (R0), and within observations (Cavagnolo et al.2009). This suggests that the cluster configurations generally produced in

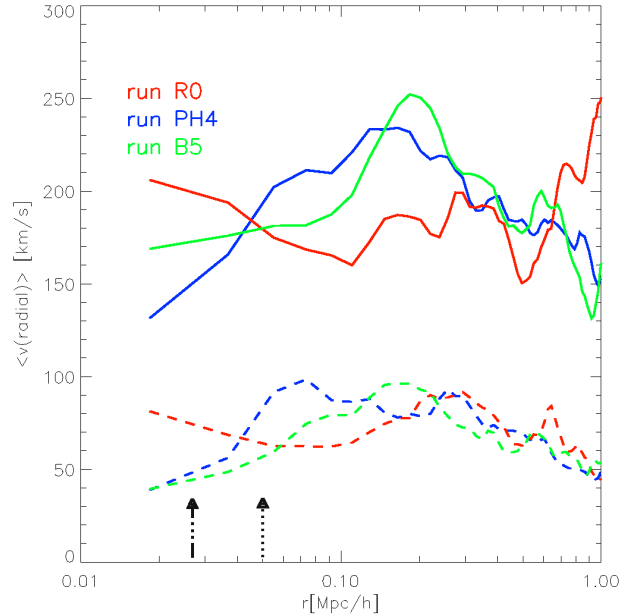


**Figure 22.** Profiles of the total radial (solid lines) and chaotic radial (dashed lines) module of velocity for run R0 (red), for run PH4 (blue) and for run B5 (green). The dotted arrow shows the softening length adopted in run R0, while the dot-dashed one shows the softening of runs PH4 and B5.

cosmological non-radiative runs may be considered, at first approximation, a viable representation of real galaxy clusters with cooling and feedback mechanisms at work. However, similar thermal distributions at  $z = 0$  may be characterized by quite different kinematic structure, depending on the different feedback mechanisms at work, leading to potentially detectable spectroscopic X-ray features. The study of other important observables not considered in this paper (such as the distribution of stars, metals, and the cluster baryon fraction) is expected to provide additional ways to discriminate between similar thermal models (e.g. Booth & Schaye 2009; Teysseier et al.2010).

Our conclusions is presently limited by the fact that we adopted so far “ad-hoc” models of pre-heating and AGN feedback, which are coupled to the simulation “by hand”, and that we focused on only two clusters (see also the Appendix). It would be interesting to investigate the same issues using a number of clusters with different masses/dynamical history.

As a final remark, we note that the mechanism which produces the entropy floor in cosmological grid simulations of non-radiative clusters can also explain the long-debated difference reported for SPH and grid run (e.g. Frenk et al.1999; O’Shea et al.2005; Tasker et al.2008; Wadsley et al.2008; Mitchell et al.2008; Springel 2010). In major merger clusters, the difference in the core entropy is set by different efficiency in the mixing of gas at the moment of the closest encounter between the clusters, as convincingly shown by Mitchell et al.(2008). In relaxed clusters, a similar mechanism works on longer time scales, due to the continuous action of subsonic chaotic motions triggered by the accretion of satellites. Any difference in the modeling of mixing in the two numerical methods can explain the presence or absence of a well defined entropy core structure. It has been shown that the presence of an artificial viscosity term in standard SPH greatly reduces the small scale mixing in a number of realistic cases, compared to standard Eulerian simulations (e.g.

Agertz et al.2007; Wadsley et al.2008; Springel 2010), and that the adoption of less viscous simulations produces entropy distributions in clusters more similar to Eulerian runs (e.g. Dolag et al.2005; Mitchell et al.2009). As shown in this work, shock heating is the leading source of entropy *production* in cluster (well beyond the role of any possible numerical artifact), while physical mixing is the reason for the *spreading* of entropy in the innermost cluster regions. The fact that mixing in SPH is usually reduced by numerical effects, fully explains while the two methods are in disagreement in the center of clusters, when mixing is maximum in grid codes, while they are found in much better agreement at larger radii (e.g. Frenk et al.1999).

Since the buoyancy in the stratified ICM is strongly dependent on the underlying entropy distribution, the above findings emphasize the need of having a suitable numerical representation of cluster cores, since this may affect also the estimated energy budget needed from non-gravitational heating mechanism, and in their efficiency in mixing/heating the surrounding Intra Cluster Medium.

## 6 ACKNOWLEDGMENTS

I am strongly indebted with my friends and advisors, G.Brunetti and C.Gheller, for the fruitful collaboration of these years, which made this work possible. I acknowledge R.Brunino, M.Nanni, F. Tinarelli and A. Tugnoli of helpful computational support at CINECA and at Radio Astronomy Institute in Bologna. I thank M.Bruggen, E.Liuzzo, K.Dolag and G.Bryan for very useful technical discussions. I thank the referee of the paper, Tom Theuns, for his constructive suggestions and comments, which helped improving the quality of this work. I acknowledge partial support through grant ASI-INAF I/088/06/0 and PRIN INAF 2007/2008, and the usage of computational resources under the CINECA-INAF 2008-2010 agreement and the 2009 Key Project “Turbulence, shocks and cosmic rays electrons in massive galaxy clusters at high resolution”.

## REFERENCES

Abel, T. 2010, arXiv:1003.0937  
 Ascasibar Y., Markevitch M., 2006, ApJ, 650, 102  
 Bialek, J. J., Evrard, A. E., & Mohr, J. J. 2001, ApJ, 555, 597  
 Bird, J., Martini, P., & Kaiser, C. 2008, ApJ, 676, 147  
 Bîrzan, L., Rafferty, D. A., McNamara, B. R., Wise, M. W., & Nulsen, P. E. J. 2004, ApJ, 607, 800  
 Bîrzan, L., McNamara, B. R., Nulsen, P. E. J., Carilli, C. L., & Wise, M. W. 2008, ApJ, 686, 859  
 Borgani, S., Governato, F., Wadsley, J., Menci, N., Tozzi, P., Quinn, T., Stadel, J., & Lake, G. 2002, MNRAS, 336, 409  
 Borgani, S., Finoguenov, A., Kay, S. T., Ponman, T. J., Springel, V., Tozzi, P., & Voit, G. M. 2005, MNRAS, 361, 233  
 Booth, C. M., & Schaye, J. 2009, MNRAS, 398, 53  
 Brighenti, F., & Mathews, W. G. 2003, ApJ, 587, 580  
 Burns J. O., Hallman E. J., Gantner B., Motl P. M., Norman M. L., 2008, ApJ, 675, 1125  
 Brüggen, M., & Kaiser, C. R. 2002, Nat., 418, 301  
 Brüggen, M., Heinz, S., Roediger, E., Ruszkowski, M., & Simionescu, A. 2007, MNRAS, 380, L67  
 Bryan G. L., Norman M. L., Stone J. M., Cen R., Ostriker J. P., 1995, CoPhC, 89, 149  
 Cavaliere, A., Menci, N., & Tozzi, P. 1997, ApJ, 484, L21

Cavagnolo, K. W., Donahue, M., Voit, G. M., & Sun, M. 2009, ApJs, 182, 12  
 Churazov, E., Forman, W., Jones, C., Boehringer, H. 2000, A&A, 356, 788  
 Dalla Vecchia, C., Bower, R. G., Theuns, T., Balogh, M. L., Mazzotta, P., & Frenk, C. S. 2004, MNRAS, 355, 995  
 David L. P., Forman W., Jones C., 1991, ApJ, 380, 39  
 David, L. P., Jones, C., Forman, W., Nulsen, P., Vrtilik, J., O’Sullivan, E., Giacintucci, S., & Raychaudhury, S. 2009, ApJ, 705, 624  
 De Young, D. S. 2003, MNRAS, 343, 719  
 De Young, D. S. 2010, ApJ, 710, 743  
 Dolag, K., Vazza, F., Brunetti, G., & Tormen, G. 2005, MNRAS, 364, 753  
 Donahue, M., Horner, D. J., Cavagnolo, K. W., & Voit, G. M. 2006, ApJ, 643, 730  
 Dubois, Y., Devriendt, J., Slyz, A., & Teyssier, R. 2010, arXiv:1004.1851  
 Dunn, R. J. H., & Fabian, A. C. 2006, MNRAS, 373, 959  
 Evrard A. E., Henry J. P., 1991, ApJ, 383, 95  
 Evrard A. E., Henry J. P., 1991, tpsu.rept, 127  
 Fabian A. C., 1994, ARA&A, 32, 277  
 Frenk, C. S., et al. 1999, ApJ, 525, 554  
 Fryxell, B., et al. 2000, ApJs, 131, 273  
 Giacintucci, S., et al. 2008, ApJ, 682, 186  
 Giodini, S., et al. 2010, ApJ, 714, 218  
 Gitti, M., O’Sullivan, E., Giacintucci, S., David, L. P., Vrtilik, J., Raychaudhury, S., & Nulsen, P. E. J. 2010, ApJ, 714, 758  
 Gu, M., Cao, X., & Jiang, D. R. 2009, MNRAS, 396, 984  
 Guo, F., & Mathews, W. G. 2010, arXiv:1004.2258  
 Haardt F., Madau P., 1996, ApJ, 461, 20  
 Heinz, S., Brüggen, M., Young, A., & Levesque, E. 2006, MNRAS, 373, L65  
 Hockney, R. W., & Eastwood, J. W. 1981, Computer Simulation Using Particles, New York: McGraw-Hill, 1981,  
 Iapichino L., Niemeyer J. C., 2008, MNRAS, 388, 1089  
 Kaiser N., 1991, ApJ, 383, 104  
 Katz N., White S. D. M., 1993, ApJ, 412, 455  
 Kay, S. T., da Silva, A. C., Aghanim, N., Blanchard, A., Liddle, A. R., Puget, J.-L., Sadat, R., & Thomas, P. A. 2007, MNRAS, 377, 317  
 Lapi A., Cavaliere A., Menci N., 2005, ApJ, 619, 60  
 Lin, W. P., Jing, Y. P., Mao, S., Gao, L., & McCarthy, I. G. 2006, ApJ, 651, 636  
 Liuzzo, E., Taylor, G. B., Giovannini, G., & Giroletti, M. 2009, A&A, 501, 933  
 Lloyd-Davies E. J., Ponman T. J., Cannon D. B., 2000, MNRAS, 315, 689  
 McCarthy I. G., et al., 2007, MNRAS, 376, 497  
 McCarthy, I. G., et al. 2009, arXiv:0911.2641  
 Merlin, E., Buonomo, U., Grassi, T., Piovani, L., & Chiosi, C. 2010, A&A, 513, A36  
 Mitchell, N. L., McCarthy, I. G., Bower, R. G., Theuns, T., & Crain, R. A. 2009, MNRAS, 395, 180  
 Norman, M. L., & Bryan, G. L. 1999, The Radio Galaxy Messier 87, 530, 106  
 Norman M. L., Bryan G. L., Harkness R., Bordner J., Reynolds D., O’Shea B., Wagner R., 2007, arXiv, 705, arXiv:0705.1556  
 O’Neill, S. M., & Jones, T. W. 2010, ApJ, 710, 180  
 O’Shea, B. W., Nagamine, K., Springel, V., Hernquist, L., & Norman, M. L. 2005, ApJ, 160, 1  
 Parrish, I. J., & Quataert, E. 2008, ApJ, 677, L9

Pearce, F. R., Thomas, P. A., Couchman, H. M. P., & Edge, A. C. 2000, *MNRAS*, 317, 1029

Ponman T. J., Cannon D. B., Navarro J. F., 1999, *Natur*, 397, 135

Poole G. B., Babul A., McCarthy I. G., Sanderson A. J. R., Fardal M. A., 2008, *MNRAS*, 391, 1163

Price, D. J. 2008, *Journal of Computational Physics*, 227, 10040

Ricker, P. M., & Sarazin, C. L. 2001, *ApJ*, 561, 621

Ritchie B. W., Thomas P. A., 2002, *MNRAS*, 329, 675

Robertson, B. E., Kravtsov, A. V., Gnedin, N. Y., Abel, T., & Rudd, D. H. 2010, *MNRAS*, 401, 2463

Romeo, A. D., Sommer-Larsen, J., Portinari, L., & Antonuccio-Delogu, V. 2006, *MNRAS*, 371, 548

Rossetti M., Molendi S., 2010, *A&A*, 510, A83

Ruszkowski, M., Enßlin, T. A., Brügggen, M., Heinz, S., & Pfrommer, C 2007, *MNRAS*, 378, 662

Ruszkowski, M., & Oh, S. P. 2010, *ApJ*, 713, 1332

Ryu, D., Ostriker, J. P., Kang, H., & Cen, R. 1993, *ApJ*, 414, 1

Ryu D., Kang H., Hallman E., Jones T. W., 2003, *ApJ*, 593, 599

Sanders, J. S., Fabian, A. C., & Taylor, G. B. 2009, *MNRAS*, 396, 1449

Scannapieco, E., & Brügggen, M. 2008, *ApJ*, 686, 927

Scannapieco, E., & Brügggen, M. 2010, *MNRAS*, 583

Schwarzschild, M. 1959, *Ap J.*, 130,345.

Sijacki, D., & Springel, V. 2006, *MNRAS*, 366, 397

Sijacki, D., Springel, V., Di Matteo, T., & Hernquist, L. 2007, *MNRAS*, 380, 877

Sijacki, D., Pfrommer, C., Springel, V., & Enßlin, T. A. 2008, *MNRAS*, 387, 1403

Springel V., 2010, *MNRAS*, 401, 791

Springel V., 2010, *MNRAS*, 401, 791

Tasker, E. J., Brunino, R., Mitchell, N. L., Michielsen, D., Hopton, S., Pearce, F. R., Bryan, G. L., & Theuns, T. 2008, *MNRAS*, 390, 1267

Teyssier, R., Moore, B., Martizzi, D., Dubois, Y., & Mayer, L. 2010, arXiv:1003.4744

Tozzi P., Norman C., 2001, *ApJ*, 546, 63

Valdarnini, R. 2002, *ApJ*, 567, 741

Vazza, F., Brunetti, G., Kritsuk, A., Wagner, R., Gheller, C., & Norman, M. 2009, *A&A*, 504, 33

Vazza, F., Gheller, C., & Brunetti, G. 2010, *A&A*, 513, A32

Vazza F., Brunetti G., Gheller C., Brunino R., 2010, arXiv, arXiv:1003.5658

Voit, G. M., Kay, S. T., & Bryan, G. L. 2005, *MNRAS*, 364, 909

Wadsley, J. W., Veeravalli, G., & Couchman, H. M. P. 2008, *MNRAS*, 387, 427

White R. E., III, 1991, *ApJ*, 367, 69

Wise, M. W., McNamara, B. R., Nulsen, P. E. J., Houck, J. C., & David, L. P. 2007, *ApJ*, 659, 1153

Woodward P., Colella P., 1984, *JCoPh*, 54, 115

Worrall, D. M. 2009, *A&Ar*, 17, 1

Xu, H., Li, H., Collins, D. C., Li, S., & Norman, M. L. 2009, *ApJL*, 698, L14

Younger, J. D., & Bryan, G. L. 2007, *ApJ*, 666, 647

Yoshikawa, K., Jing, Y. P., & Suto, Y. 2000, *ApJ*, 535, 593

Zanni, C., Murante, G., Bodo, G., Massaglia, S., Rossi, P., & Ferrari, A. 2005, *A&A*, 429, 399

ZuHone, J. A., Markevitch, M., & Johnson, R. E. 2009, arXiv:0912.0237

ZuHone J., 2010, arXiv, arXiv:1004.3820

## 7 APPENDIX

Cluster mergers may boost shock heating and mixing motions in the ICM for several Gyrs (e.g. Ricker & Sarazin 2001), significantly changing the physical entropy generation in a cluster with a dynamical evolution different than the relaxed case explored in the main part of the paper.

We present here some complementary tests on the entropy distribution of a major merger cluster of final mass  $M \approx 2.1 \cdot 10^{14} M_{\odot}/h$ . The bulk of the total mass of this cluster is assembled in a major merger at  $z = 0.85$ , with an approximate mass ratio of  $M_1/M_2 \sim 3$  between the colliding halos. Only a subsample of the re-simulations presented in the main part of the paper were repeated with this cluster; the parameters of the tests run in this case are listed in Table 7 (all the cosmological parameter are as in Sec.3.1). The non radiative simulation of this cluster produces a flat entropy core with  $S \sim 80-90 keV cm^2$  for  $r < 100 kpc/h$ , similar to the non-radiative fiducial run (run R0, Sec.3.2).

The adoption of the additional mesh refinement based on velocity jumps (run A2) causes a net increase of the internal entropy compared with the more standard mesh refinement strategy based on gas/DM over-density (A1), as shown in Sec.3.2. The role of the gravitational softening is found to be more important in this major merger cluster, compared to the relaxed cluster studied in the main part of the paper: the adoption of a larger softening ( $50 kpc/h$ , run A3) produces an entropy core larger by  $\sim 20$  per cent compared to a smaller softening ( $25 kpc/h$ , run A2). This stresses the higher importance of having a good resolution for the computation of gravitational forces in the case of violent oscillations of the gravitational potential driven in a merger event, which may generate an amount of extra-entropy production of numerical origin.

The adoption of radiative cooling (in the case of standard refinement, C1, or with the velocity-based refinement, C2) causes a very similar trend as in the case of the relaxed cluster explored in the paper, with the onset of catastrophic cooling for  $r < 200 kpc/h$ . This shows that, at least for this *early* major merger ( $z \sim 0.85$ ), the action of intense heating from merger shocks is not effective in destroying the forming cooling region, somewhat at variance with other works with Eulerian simulations (e.g. Burns et al.2008).

To spare computational time, most of the runs with non-gravitational heating were performed only with the standard refinement scheme. A uniform pre-heating of  $S_0 = 100 keV cm^2$  at  $z = 10$  (run PH2) is ineffective to stop the catastrophic cooling for  $r < 50 kpc/h$ ; however when applied to this major merger system it results in a significantly higher inner entropy value compared to the relaxed system studied in the main part of the paper (Sec.4.2.1). A pre-heating of  $S_0 = 200 keV cm^2$  (PH3) on the other hand almost perfectly recover the entropy distribution of the non-radiative run (PH3) for the merger cluster.

Runs with pre-heating of  $S_0 = 100 keV cm^2$  and AGN feedback were produced for the jets energy of  $\epsilon_{jet} = 2 \cdot 10^{57} ergs$  (run J1) and  $\epsilon_{jet} = 10^{58} ergs$ . The profile of the J1 run is very similar to what obtained for the relaxed cluster of the paper; the profile with a higher AGN energy results in a flat entropy profile at  $\sim 130 keV cm^2$  for  $r < 200 kpc/h$ . Finally, we re-simulated run J2 adopting the velocity based refinement (run J3), finding still a very flat profile inside  $r < 200 kpc/h$ , and a  $\sim 50$  per cent larger entropy in the center. According to the assumed jet energy, our re-simulations with cooling, pre-heating and AGN feedback can thus provide an acceptable match with one of the two classes of the bimodal entropy distribution reported for the CHANDRA observations of Cavagnolo et al.(2009).

**Table 2.** Main characteristics of the performed runs (as in Tab.2). In the last row, the assumed pre-heating background is  $S_0 = 100 \text{ keV cm}^2$  and the thermal energy of the jets is  $2 \cdot 10^{57} \text{ ergs}$

ID	Max Res. [kpc/h]	soft. [kpc/h]	AMR	note
A1	25	25	D	non-radiative
A2	25	25	DV	non-radiative
A3	25	50	DV	non-radiative
C1	25	25	D	cooling
C2	25	25	DV	cooling
PH2	25	25	D	cool.+PH( $100 \text{ keV cm}^2$ )
PH3	25	25	D	cool.+PH( $200 \text{ keV cm}^2$ )
J1	25	25	D	cool.+PH+J( $2 \cdot 10^{57} \text{ ergs}$ )
J2	25	25	D	cool.+PH+J( $10^{58} \text{ ergs}$ )
J3	25	25	DV	cool.+PH+J( $10^{58} \text{ ergs}$ )

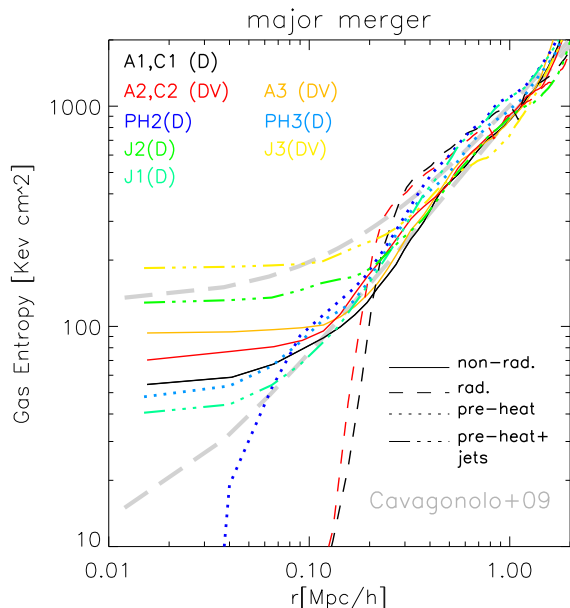


**Figure 23.** Profiles of the gas entropy in the major merger run. The additional long dashed line show the bimodal gas entropy distribution from CHANDRA observations (Cavagnolo et al.2009).

In Fig.7 we show the time evolution for three snapshots of run C1, J2 and J3, showing the X-ray bolometric luminosity for a region of  $\sim 1.8 \times 2.2 \text{ Mpc/h}$  per side and thickness  $25 \text{ kpc/h}$ , around the epoch of the major merger. Comparing C1 to J2, we show how the action of AGN feedback removes the central gas condensation within the cooling region in a few  $\sim 10 \text{ Myr}$ . Run J3 emphasizes the role played by the mesh refinement strategy on the expanding shocks driven by the (almost contemporary) AGN burst and the major merger. We also note how at least one inflated “bubble” can survive for a few time steps after the injection, due to the reduced numerical mixing in the implemented mesh refinement strategy.

The above tests suggest that the most important findings reported in the main body of the article are general, since they apply to clusters with a similar mass but two completely different dynamical histories. However the efficiency of the extra-heating models applied to radiative runs may depend on the dynamical history of the host cluster, and further studies are needed to estimate the global efficiency of the proposed scenarios in a statistical sense.

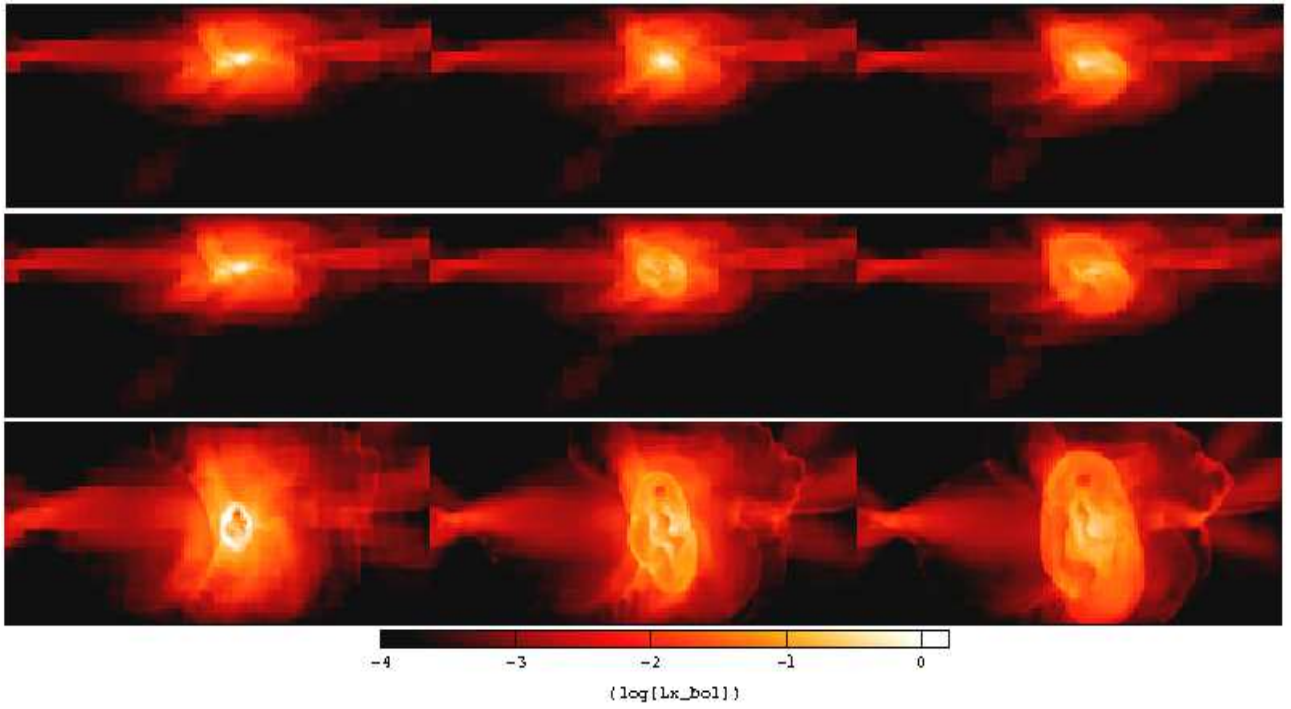


**Figure 24.** Maps for the evolution of the X-ray bolometric luminosity for slices of  $1.8 \times 2.2 Mpc/h$  and depth  $25 kpc/h$  for the major merger cluster studied in the Appendix, at  $z = 0.9$ ,  $z = 0.85$  and  $z = 0.81$ . The top panels are for the pure cooling run (C1), the middle panels are run J1 with cooling, pre-heating ( $S = 100 keV cm^2$  at  $z = 10$ ) and AGN feedback ( $\epsilon_{jet} = 10^{58} erg/s$ ), while the bottom panel are for a re-simulation with the same setup, but mesh refinement triggered by velocity jump (run J3).